Earth's Future

RESEARCH ARTICLE
10.1029/2021EF002298

Key Points:

- In 21st century simulations with fixed present-day aerosol emissions, air quality worsens in many parts of South America, Africa and Asia
- Surface concentrations of sulfate, black carbon and primary organic matter increase globally, while secondary organic matter declines
- Greenhouse gas driven changes in rainfall frequency, temperature, and moisture availability impact the production and removal of aerosols

Supporting Information:

Supporting Information may be found in the online version of this article.

Correspondence to:

G. J. Kooperman,
kooperman@uga.edu

Citation:

Banks, A., Kooperman, G. J., & Xu, Y. (2022). Meteorological influences on anthropogenic $PM_{2.5}$ in future climates: Species level analysis in the Community Earth System Model v2. *Earth's Future*, *10*, e2021EF002298. https://doi.org/10.1029/2021EF002298

Received 1 JUL 2021
Accepted 8 DEC 2021

Author Contributions:

Conceptualization: Alison Banks, Gabriel J. Kooperman, Yangyang Xu
Formal analysis: Alison Banks, Gabriel J. Kooperman
Funding acquisition: Gabriel J. Kooperman
Methodology: Alison Banks, Gabriel J. Kooperman, Yangyang Xu
Resources: Gabriel J. Kooperman
Supervision: Gabriel J. Kooperman
Validation: Alison Banks

Meteorological Influences on Anthropogenic $PM_{2.5}$ in Future Climates: Species Level Analysis in the Community Earth System Model v2

Alison Banks[1], **Gabriel J. Kooperman**[1], **and Yangyang Xu**[2]

[1]Department of Geography, University of Georgia, Athens, GA, USA, [2]Department of Atmospheric Sciences, Texas A&M University, College Station, TX, USA

Abstract Biomass and fossil fuel burning impact air quality by injecting fine particulate matter ($PM_{2.5}$) and its precursors into the atmosphere, which poses serious threats to human health. However, the surface concentration of $PM_{2.5}$ depends not only on the magnitude of emissions, but also secondary production, transport, and removal. For example, in response to greenhouse gas driven warming, meteorological conditions that govern aerosol removal, primarily through rainfall and wet deposition, could shift in pattern, frequency, and intensity. This climate change driven process can impact air quality even without changes in aerosol emissions. In this experiment, we conduct new simulations by fixing aerosol emissions at present-day levels in the Community Earth System Model Version 2, but increasing greenhouse gases through the 21st century. In our results, the changes in patterns and intensity of $PM_{2.5}$ are found to be associated with precipitation (via aerosol removal), temperature (via secondary organic aerosol (SOA) formation), and moisture and clouds (via sulfate production). A decrease in wet day frequency (~1.2% global mean) contributes to increases in the surface concentrations of black carbon, primary organic matter, and sulfate in many regions. This is offset in some regions by an upward vertical shift in the level where SOA forms, which contributes to higher column burden but lower surface concentration. These results highlight a need, using a variety of modeling tools, to continually reassess aerosol emissions regulations in response to anticipated climate changes.

1. Introduction

The World Health Organization estimates that 4.2 million deaths each year are associated with exposure to fine particulate matter aerosol ($PM_{2.5}$; aerosol particles with diameter less than 2.5 micrometers), which is capable of penetrating lung membranes (WHO, 2016). Fortunately, direct anthropogenic emissions are projected to decrease globally as countries implement better air quality policies through the 21st century (O'Neill et al., 2016). However, in addition to direct emissions, many atmospheric processes can influence the transport and removal of particle pollutants from the atmosphere. Likewise, meteorological conditions can impact the production and secondary formation of some aerosol particles. Some recent studies show that projected increases in $PM_{2.5}$-related mortality rates have been linked to changes in these physical climate conditions in response to future greenhouse gas warming (Park et al., 2020; Silva et al., 2016, 2017), but the impacts vary regionally. For example, South Asian meteorological drivers may contribute to better air quality (Wu et al., 2019), while pollution in east China is exacerbated by 21st century warming (Chen et al., 2019; Feng et al., 2020), even in experiments with emissions held constant at present-day values in those regions (Hong et al., 2019). To better understand the drivers of future changes in air quality and associated human health impacts, it is thus critical to assess how the sinks, as well as sources, of aerosol may change, at a detailed regional and species level.

Precipitation has a major role in removing atmospheric pollutants by wet deposition through the processes of in- and below-cloud scavenging, in which aerosol particles are collected by rain droplets and deposited with precipitation that reaches the surface (Poeschl, 2006). This is a critical, natural process that removes pollutants from the atmosphere and can lead to improved air quality conditions. Global modeling results by Wang et al. (2021) demonstrate that it is the frequency of light-to-moderate rates that have the primary control on aerosol removal. In recent decades, regional observations from both ground and satellite networks have quantified aerosol-precipitation relationships (e.g., Hoelzemann et al., 2009; Keene et al., 2015; Lynch et al., 2000; Sickles & Shadwick, 2007; Vet et al., 2014). Using a combination of satellite observations and a global chemical transport model, Hou (2018) found that the frequency of precipitation had a higher impact on aerosol burden (i.e., mass

Writing – original draft: Alison Banks, Gabriel J. Kooperman
Writing – review & editing: Alison Banks, Gabriel J. Kooperman, Yangyang Xu

of aerosol in a column of the atmosphere) than precipitation intensity. Decreases in precipitation frequency contributed to 10% or higher increases in the lifetime of aerosol in some regions over the last 30 years. During some heavy pollution events, the occurrence of precipitation and wet removal can be a dominant sink of aerosol (e.g., Yang et al., 2020; Zhang et al., 2019), but the overall role of precipitation during individual events can depend on other factors, such as atmospheric stability (e.g., Roldán-Henao et al., 2020).

As greenhouse gas concentrations are expected to continue to increase through the 21st century, precipitation characteristics are projected to change in ways that may influence the removal of aerosol particles and the efficiency of atmospheric cleansing events (Allen & Soden, 2008). In particular, the frequency of intense precipitation events is projected to increase, while the frequency of light-to-moderate events is projected to decrease, leading to an overall decrease in total precipitation frequency on a global-scale (Allen & Soden, 2008; Kooperman et al., 2016a; O'Gorman & Schneider, 2009; Pendergrass & Hartmann, 2014a, 2014b; Sun, 2007). Global patterns of precipitation are also projected to change, such as the wet-get-wetter—dry-get-drier paradigm (Held & Soden, 2006), weakening and expansion of the Hadley circulation (Seidel et al., 2008), and poleward shift in storm tracks (Yin, 2005). These precipitation changes have been linked to a projected increase in global aerosol burden in Earth system model simulations with future climate conditions, but with aerosol emissions specifically fixed at present-day levels (e.g., Allen et al., 2015). Surface aerosol concentrations are also shown to increase more in some regions due to stronger reductions in precipitation frequency in response to global warming (Xu & Lamarque, 2018).

In addition to precipitation, changes in some other meteorological conditions can impact the production of aerosol in the atmosphere, including temperature, moisture and clouds. The production of particulate matter, either onto existing or new particles, involves the oxidation of precursor gases such as VOCs, SO_2, and NO_x, which contribute to the mass of secondary organic aerosol (SOA) and sulfate (SO_4) aerosol (Eatough et al., 1994; Ervens et al., 2011; Kroll et al., 2006). Formation of SO_4 can occur in both gas- and aqueous-phase, the latter of which depends on moisture and cloud water availability (Scott & Hobbs, 1967). SOA production is rather complex, involving formation mechanisms that are specific to different organic compounds, and their dependence on temperature (saturation vapor pressure) and other climate/chemical conditions (Hallquist et al., 2009; Shrivastava et al., 2017). In addition to phase transitions of SOA in the atmosphere, climate changes can also influence natural emission rates of SOA precursors. For example, in a global climate model with an explicit treatment of SOA, biogenic isoprene emissions were found to increase by 18% as a result of higher temperatures, contributing to a 25% increase in SOA burden (Lin et al., 2016). Although the increase in burden was largely offset by land-use and anthropogenic emissions changes, leading to a smaller overall change with all factors considered.

In this study, with state-of-art modeling tools, we isolate the aerosols changes driven by climate change induced atmospheric changes from those due to changes in aerosol and precursor gas emissions by simulating the 21st century with increasing greenhouse gases but with aerosol emissions held at the present-day rates. These results are compared to a matching simulation with both time evolving greenhouse gas and aerosol emissions changes. The model and simulations are described in Section 2, followed by a comparison to observations in Section 3, analysis of future changes in Section 4, and a summary of the major findings in Section 5.

2. Model and Methods

In this study, the National Center for Atmospheric Research's Community Earth System Model (CESM2.1.1; Danabasoglu et al., 2020), with aerosol treatment through the Community Atmosphere Model (CAM6; Neale et al., 2012; Bogenschutz et al., 2018) component, is used to investigate the connection between climate change and air quality. CAM6 has an interactive representation of aerosol processes, which includes direct emissions of particulate matter and precursor gases for SO_4 and SOA (Liu et al., 2012, 2016), described in more detail below. Aerosol mass and number concentrations are linked to cloud processes through a two-moment cloud-microphysics scheme, which influences droplet/ice formation (Gettelman & Morrison, 2008). Aerosols are transported by circulation and removed by dry and wet deposition, the latter of which includes removal through in- and below-cloud scavenging by precipitation (Liu et al., 2012). They can directly impact clear-sky radiative calculations through the Rapid Radiative Transfer Model for GCMs (Iacono et al., 2008), and are linked to atmospheric processes in CAM6 (e.g., cloud microphysics and radiation), as well as surface models, and thus impact other climate-system processes. Within CESM2.1.1, CAM6 can be run coupled to interactive ocean, sea-ice, and

land-surfaces models, which reproduces large-scale patterns of variability, such as ENSO, for the present-day climate. The coupled model can also be run for a suite of future scenarios (Danabasoglu et al., 2020).

In CAM6, aerosols are represented by a prognostic modal aerosol scheme (the Modal Aerosol Module, MAM4), which tracks the mass mixing ratio of six species (i.e., sulfate, black carbon (BC), primary organic aerosol, and SOA, sea salt and dust) and number concentration in four modes (Ghan et al., 2012; Liu et al., 2012, 2016). The internally mixed modes (i.e., average chemical and physical properties based on the mass of all species within) include "Aitken", "accumulation", and "coarse" in order of smallest to largest size range. In addition, primary organic matter and BC aerosol are initially emitted into a fourth "primary carbon" mode that ages into the accumulation mode. Following Xu and Lamarque (2018), we use the fine modes of the modal aerosol module (i.e., Aitken and Accumulation) as a proxy for surface $PM_{2.5}$, and include BC, POM, SOA and SO_4 aerosol. With the exception of dust and sea salt emitted from natural sources, primary emissions of aerosol particles and precursors gases are prescribed with a time-varying annual cycle from the Community Emissions Data System (CEDS) (Smith et al., 2015).

In addition to the primary emissions of aerosol, SOA and SO_4 in MAM4 form in the atmosphere as a result of precursor gas emissions and as a function of atmospheric conditions. For SOA, a lumped single gas-phase species (i.e., SOAG) is emitted, which is based on an offline calculation of VOC oxidation with fixed mass yields from the Model for Ozone and Related Chemical Tracers (MOZART) (Neale et al., 2012; Tilmes et al., 2019). Note that, unlike Lin et al. (2016), the emissions of SOAG are prescribed in CESM2, so their changes with climate will not be assessed here, but the subsequent impact of climate on SOA formation, transport and removal can be isolated, which is the focus of this study. In particular, SOA formation depends on temperature (governing the saturation vapor pressure of SOA) and the current concentration of organic aerosol present within each mode, which influences the partial pressure of SOAG. Therefore, changes in temperature and atmospheric circulation (via the transport of SOAG) can both impact how much and where in the atmosphere SOA forms.

Of the six aerosol species in MAM4, SO_4 is unique in that its sources are from direct emissions as well as secondary production, which occurs through both aqueous chemistry and gas-phase reactions. Gas-phase sulfur emissions include natural (e.g., volcanic SO_2 and oceanic DMS) and some industrial processes, which are converted to SO_4 aerosol (forming new particles and condensation on existing particles) using reaction rate coefficients and prescribed monthly averaged oxidant concentrations from the offline MOZART runs (Emmons et al., 2020; Lamarque et al., 2010; Neale et al., 2012; Tie et al., 2001). In the gas-phase reactions, SO_2 and DMS are converted into SO_4 by OH via oxidation, which includes the conversion of DMS to SO_2, as well as H_2O_2 production and destruction. Aqueous production involves the oxidation of SO_2 in cloud droplets, which depends on characteristics of clouds (e.g., cloud fraction and liquid water content), cloud droplet concentration, and droplet pH (ion concentration of SO_4), and thus is subject to projected changes in hydrological processes.

In this study, we analyze CESM2 simulations based on the Shared Socioeconomic Pathways 5-85 scenario (SSP5-85), which represents fossil-fuel based economic growth (i.e., high greenhouse gas concentrations; O'Neill et al., 2016) for the 21st century (2016–2098). CESM2 is run in a fully coupled configuration (i.e., interactive atmosphere ocean, sea-ice, and land) and CAM6 uses a finite volume dynamical core at a horizontal resolution of 1.9° latitude by 2.5° longitude. In the SSP5-85 scenario, particulate air pollution is greatly managed in many countries such that aerosol emissions generally decrease over the 21st century, yet greenhouse gas emissions continue to rise. In comparison to the standard SSP5-85 experiment design (hereafter referred to as SSP585-Full), we also construct a separate scenario in which aerosol emissions are held fixed at the present-day rates (hereafter referred to as SSP585-Fixed). In this simulation, the greenhouse gas concentrations and land-use change follow the SSP5-85 scenario, but all prescribed aerosol emissions (and related precursor emissions, e.g., SO_2) repeat an annual cycle fixed at 2010 values. Fixed emissions apply to the four species of SO_4, POM, BC, and SOA, but not dust and sea-salt, which are interactively generated in the model based on simulated meteorological conditions.

By isolating aerosol emissions in this set of paired experiments, this study is able to assess the meteorological influences of GHG-driven climate changes on air quality in the absence of changes in their sources. For example, Lin et al. (2016) noted an 18% increase in isoprene emissions, but a 25% increase in the SOA burden, implying that changes in climate also plays a role in aerosol secondary production and removal processes. The approach here will help shed light on the relative role of removal processes. This is similar to the experiment used in Xu and Lamarque (2018) but updated here with latest model and scenarios (CESM2 and CMIP6 SSP5-85), with

a focus on individual species to better understand their distinct drivers and spatial patterns. Additionally, this experiment design differs from others that used a time-slice approach (Allen et al., 2015; Lamarque et al., 2013), in which the surface conditions (sea-surface temperatures and sea-ice cover) were prescribed for present-day and future from simulations that had originally included transient aerosol emissions. Here aerosol emissions are intentionally fixed at present-day levels while the climate system continues to evolve through the 21st century; therefore, aerosols do not directly impose a signature on the climate due to their anticipated change in emissions (e.g., Wang et al., 2017).

3. Observational Analysis

Before discussing the projected changes in climate conditions and aerosol concentrations, we first assess the fidelity of CESM2 in representing their spatial patterns and magnitudes in the present-day climate. Aerosol Optical Depth (AOD) data is taken from the Modern-Era Retrospective analysis for Research and Applications (MERRA-2) and is provided by the Observations for Model Comparison Project (Obs4MIP; Teixeira et al., 2014). MERRA-2 AOD measurements are assimilated from satellite observations with similar results to MODIS and AERONET optical depth measurements (Gueymard & Yang, 2020; Shi et al., 2019). The MERRA-2 data spans a 20-year time period from 2000 to 2020 (Bosilovich et al., 2019), which are compared to the first 20-year (simulations years 2016–2035) of the SSP585-Fixed simulation (Figure S1 in the Supporting Information S1) driven by present-day aerosol emissions. Similarly, we compare a nineteen-year period (1998–2016) of surface $PM_{2.5}$ observations, which exclude dust and sea-salt, to our matching analysis from the SSP585-Fixed simulation. This data product is based on a combination of satellite observations (MODIS, MISR, and SeaWiFS) and are derived using geographically weighted regression analysis. The data is developed by the Center for International Earth Science Information Network, and obtained from the NASA Socioeconomic Data and Applications Center (van Donkelaar et al., 2018).

AOD measures the extinction coefficient of aerosol particles as a vertically integrated quantity and provides information about the total aerosol burden in the atmosphere. In general, the overall magnitude and spatial pattern of AOD in CESM2 compare reasonably well to MERRA-2, but with some regional biases (Figure S1 in the Supporting Information S1). When comparing the observed and simulated AOD, the generally high values over northern Africa and Asia are represented in CESM2, but with a high (low) bias over northeast (northwest) Africa and a low (high) bias over eastern China (Tibetan plateau). Moderate magnitudes over South America, Australia and parts of Europe are also comparable to MERRA-2, but the northern high-latitudes are generally underestimated relative to observations. Over the ocean, CESM2 captures the outflow in the North Atlantic associated with Saharan dust and moderate values due to sea-salt emissions over the Southern Ocean. CESM2 also captures surface $PM_{2.5}$ (Figure S1c in the Supporting Information S1) well compared to observations (Figure S1d in the Supporting Information S1) over land. Surface fine aerosol (excluding dust and sea-salt) is present over equatorial continents with strong concentrations in India, east Asia, central Africa and similarly located over South America.

Likewise, we use a 20-year period from 1996 to 2015 of precipitation observations from the Global Precipitation Climatology Project (GPCP) 1 Degree Daily (1DD) dataset, provided by NOAA (Huffman et al., 2016; Pendergrass & National Center for Atmospheric Research Staff, 2016). The long record and daily resolution of the precipitation data allows for a comparison of the annual average (Figure S2a and S2b in the Supporting Information S1) and frequency (Figure S2c and S2d in the Supporting Information S1). CESM2 captures the overall patterns of the annual mean and daily frequency of precipitation compared to GPCP 1DD (Figure S2 in the Supporting Information S1). Annual precipitation rates are similar in scale, and the largest values are focused in the tropics in both the SSP585-Fixed simulation and GPCP 1DD. Moderate to high values are also captured over warm ocean currents in the northern hemisphere, the northwest United States, and the Southern Ocean. However, CESM2 continues to suffer from a "double ITCZ" pattern and the magnitude in the ITCZ is slightly overestimated. Similarly, the pattern of wet day frequency (threshold $\geq$ 1 mm day^{-1}) is well represented in CESM2, highlighting the same regions as observed, with high frequency over the ITCZ and mid-latitude oceans, and low frequency over the subtropics and desert regions. However, like many modern ESMs, CESM2 still has a tendency to rain too frequently (Akinsanola et al., 2020). This frequency bias tends to reduce with a higher wet-day threshold (Polade et al., 2014), which may be more relevant to aerosol removal. Nevertheless, such an overestimation of frequency may impact the interpretation of results, which are discussed next.

4. Results

The analysis of 21st century changes presented below is based on comparisons between 20-year time periods at the present-day (2016–2035) and end-of-century (2079–2098). Unless otherwise stated, the global maps show the annual climatological statistics of aerosol fields (e.g., surface concentration) and meteorological conditions (e.g., surface precipitation rate). Our analysis focuses on BC, POM, SOA and SO_4 aerosol, which have fixed present-day emissions and precursor gases in the SSP585-Fixed simulation.

4.1. Changes in Total Aerosol Burden and Surface Concentrations

In order to illustrate the overall impact of holding aerosol emissions fixed at present-day rates, we first compare simulated aerosol concentrations from the SSP585-Fixed run (Figure 1, left column) with the SSP585-Full run, which includes changes in aerosol sources over the 21st century (Figure 1, right column). Most of the differences result from changes at the end of the century (2079–2098), but some initial differences emerge within the first 20 years (2016–2035, referred to as "present-day") due to the projected near-term reductions at the beginning of the SSP585-Full simulation. In particular, there are lower values of $PM_{2.5}$ and less frequent hazardous air quality days over East Asia in SSP585-Full, but other regions are similar in the two simulations (Figure S3 in the Supporting Information S1). However, toward the end of century, significant decreases in emissions in the SSP585-Full simulation lead to reductions in the burden and $PM_{2.5}$ everywhere, except a small region over western Europe and northwest Africa (Figures 1b and 1d). While in SSP585-Fixed, the burden generally increases everywhere, and $PM_{2.5}$ shows regions of both increase (e.g., Andes, Europe, and northern Asia) and decrease (e.g., Amazon). For our analysis, we focus on the four aerosol species with fixed emissions. We excluded the interactively emitted dust and sea salt, which contribute significant mass but have a relative change that is largely consistent with the four other species outside of dust source regions (Figure S4 in the Supporting Information S1).

The consistent positive change in the spatial pattern of column burden in SSP585-Fixed (Figure 1a) implies that, in the absence of emissions reductions, meteorological factors act largely to reduce the removal of aerosol from the atmosphere in the future. This induces a 9.0% increase in the global average burden and 7.9% increase in lifetime (see absolute values in Table 1), with positive contributions from all four species (4.0%, 5.1%, 9.7% and 11.4% for BC, POM, SOA and SO4 burden, respectively). Changes in fine aerosol at the surface in SSP585-Fixed (Figure 1c) have a more varied spatial pattern, suggesting changes in the vertical distribution of aerosols. In some areas the surface air quality improves with respect to $PM_{2.5}$ (e.g., Brazil and coastal East Asia), but this is accompanied by areas of increase nearby, such that a dipole pattern emerges. For example, a decrease of $PM_{2.5}$ in the Amazon is accompanied by increases to further south. Similarly, the decrease of $PM_{2.5}$ along the coast of South and East Asia is accompanied by increases to the northwest. Since aerosol emissions remain constant, this dipole pattern is largely associated with deposition and transport changes. In the global average, surface $PM_{2.5}$ increases by 1.3% (Table 1b). Overall, SO_4 has the largest contribution to global average surface increases at 9.3%. Despite a strong increase in atmospheric column burden, a reduction at the surface from SOA (−5.8%) offsets increases from other species (3.1%, 1.5% and 9.3% for BC, POM and SO_4, respectively). The species-dependent discussion will continue in the next sub-section.

In addition to prolonged exposure to long-term mean conditions, extreme events can also have serious health impacts. The World Health Organization sets the guidelines for hazardous air quality with a daily threshold of $PM_{2.5}$ at 25 $\mu g/m^3$ (WHO, 2016). In the SSP585-Fixed simulation, the percentage of these hazardous air quality days (associated with the four fixed aerosol species, i.e., POM, BC, SO_4, and SOA) increases by more than 5% in some regions through meteorological effects alone (Figure 1e), which partially offsets the overall emissions-driven decrease as projected in SSP585-Full (Figure 1f). Changes in hazardous air quality days are also consistent with regionally defined extremes of $PM_{2.5}$, such as the 99.9th percentile (Figure S5 in the Supporting Information S1), which shows broad increases in extreme air quality events over the Eurasian continent and parts of Africa. However, like the mean surface conditions, the change in the percentage of poor air quality days is not spatially uniform, with some areas of reduction (e.g., parts of South America, Central Africa, India and southern China). Instead, hazardous air quality days worsen in particular locations, intensifying over the 21st century in countries such as Bolivia, Egypt, Bangladesh, and northern China (including around populated areas such as Beijing as noted in Feng et al., 2020).

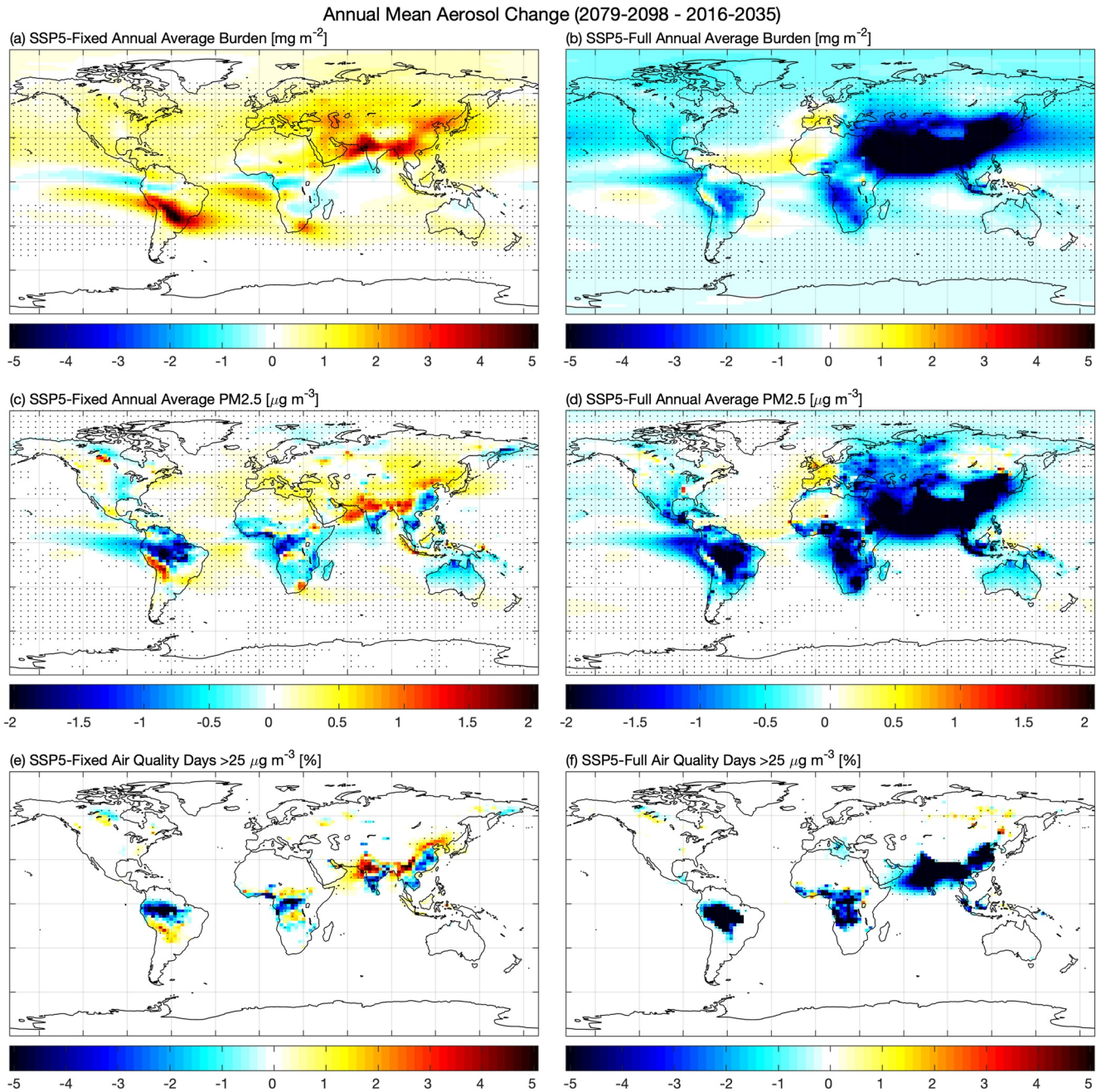

Figure 1. Measures of aerosol concentration changes [(2079–2098)−(2016–2035)] in SSP585-Fixed (left) and SSP585-Full (right) simulations. Total annual average aerosol burden (a and b) includes BC, POM, SOA, and SO_4 in all modes in units of [mg/m^2]. Annual mean $PM_{2.5}$ at the surface (c and d) includes BC, POM, SOA, and SO_4 in fine modes in units of [μg/m^3]. Hazardous air quality days (e and f) are days that exceed a 25 μg/m^3 threshold in units of [%]. Stippling on all subplots indicates statistical significance of these changes at the 99% confidence level.

Because of the often-conflicting changes spatially, in the sub-sections below we examine changes in the spatial patterns and mechanisms influencing individual species in the SSP585-Fixed simulation. BC and POM are assessed together because they have similar source regions and result from primary emissions, so concentrations are directly affected by changes in removal and transport processes. For SOA and SO_4, secondary production also contributes to changing concentrations, but in distinct ways detailed below. To understand the drivers of aerosol changes, we first depict how relevant meteorological conditions respond to climate change in this model experiment, including temperature, moisture, and precipitation.

Table 1
Area-Weighted Global Annual Averages for Aerosol Column Burden, Surface Concentration, and Lifetime (Calculated as Global Average Aerosol Burden Divided by Total Deposition or Removal) in the Fixed Aerosol Simulation (SSP585-Fixed) for Present (2016–2035) and Future (2079–2098) Conditions

	Present	Future	Change	% Change
(a) Column aerosol burden (mg/m^2)				
Total	6.11	6.66	0.55	8.97
BC	0.28	0.29	0.01	3.97
POM	1.55	1.63	0.08	5.15
SOA	1.82	2	0.18	9.72
SO_4	2.46	2.74	0.28	11.36
(b) Surface aerosol concentration (μg/m^3)				
Total	2.25	2.28	0.03	1.24
BC	0.13	0.13	0	3.13
POM	0.66	0.67	0.01	1.66
SOA	0.80	0.76	−0.05	−5.85
SO_4	0.66	0.72	0.06	9.29
(c) Aerosol lifetime (days)				
Total	4.78	5.16	0.38	7.95
BC	5.36	5.56	0.21	3.88
POM	5.96	6.26	0.3	4.98
SOA	4.21	4.61	0.41	9.63
SO_4	4.62	5.04	0.42	9.09

4.2. Changes in Large-Scale Meteorological Conditions

In SSP585-Fixed, greenhouse gas concentrations rise through the 21st century leading to a 3.1°C increase in global mean temperature (Table 2). The spatial pattern shows greater warming at northern high latitudes (>10°C) due to Arctic amplification, and higher values over land (Figure 2a). Temperature plays a key role in controlling the saturation vapor pressure of gas-phase constituents in the atmosphere, and warming can influence their condensation and the production of aerosol. Overall, moisture increases with temperature following the Clausius-Clapeyron relation (Table 2), with the largest total column increases across the tropics (Figure 2c) where present-day values are high (Figure S6c in the Supporting Information S1). Globally, the surface relative humidity changes by a small amount, but with decreases over most land areas due to greater warming and lower moisture availability (Figure 2b), with the exception of central Africa and India (Xu et al., 2020). Cloud water has a more varied spatial response (Figure 2d), with decreases over east Asia, southern Africa, northern South America and Australia, and increases over India, central Asia, Russia, central Africa and the United States. As detailed later, these changes in atmospheric moisture and cloud water can influence secondary aerosol production through aqueous-phase processes, which is relevant to SO_4 production represented in CESM2.

Changes in the characteristics of precipitation are especially relevant for aerosol removal. Global mean precipitation increases by 4.3% in SSP585-Fixed (Table 2), driven by radiative constraints associated with increasing greenhouse gas concentrations (Pendergrass & Hartmann, 2014a, 2014b). The largest increases occur across the tropics and at high latitudes, with decreases in the subtropics and over the Amazon (Figure 2e). However, the frequency of daily precipitation events may better explain aerosol wet deposition changes (a primary sink for aerosol particles) compared to the average precipitation, and the frequency tends to decrease in response to rising greenhouse gas concentrations. There is a global mean decrease in the wet day frequency of 1.2% (Table 2), with some regions decreasing by more than 15% (Figure 2f). The frequency of precipitation increases along the equator, but decreases widely across most sub-tropical and mid-latitude oceans, particularly in transition zones from climatologically dry to wet ocean regions (Figure 2f and S6f in the Supporting Information S1). Over land, the pattern of frequency change is mostly consistent with the average change, however, notable exceptions are in southeast and east Asia and the Maritime Continent where the average increases but the frequency declines. Furthermore, average precipitation is relatively unchanged in Europe and the Mediterranean, but there is a strong decrease in the frequency of rain events there.

Table 2
Area-Weighted Global Annual Averages for Climate Variables in the Fixed Aerosol Simulation (SSP585-Fixed) for Present (2016–2035) and Future (2079–2098) Conditions

	Present	Future	Change
Surface temperature [K]	288.4	291.5	3.1
Surface relative humidity [%]	77.56	77.43	−0.12
Surface specific humidity [kg/kg]	0.011	0.013	0.002
Precipitable water [kg/m^2]	26.19	32.30	6.11
Grid box cloud water [kg/m^2]	0.062	0.064	0.002
Precipitation [mm/day]	2.964	3.089	0.126
PBL height [m]	739.3	720.9	−18.4
Wet day frequency [%]	44.6	43.34	−1.2

On one hand, one may expect increases in global mean precipitation to drive more wet deposition and decrease aerosol concentrations overall, potentially improving air quality. On the other hand, global mean reductions in wet day frequency can allow aerosol to increase more before it rains, potentially worsening air quality. We assess this globally by comparing precipitation distributions with the conditional wet deposition amount distribution as a function of precipitation rate following Wang et al. (2021). As noted above, there is a small decrease in the global mean frequency of wet days (−0.6% and −1.2% when defined as >0.1 mm/day and >1 mm/day, respectively). The overall decrease is controlled by decreases for the most frequent moderate rates that occur between about 0.7 and 8 mm day^{-1} (Figure 3a), with slight increases for lighter and heavier rates. The lighter rates do not have a strong influence on wet deposition and the increased frequency for those rates occurs only over the ocean (not shown), so they do not impact aerosol removal significantly. However, despite the overall decrease in frequency, global

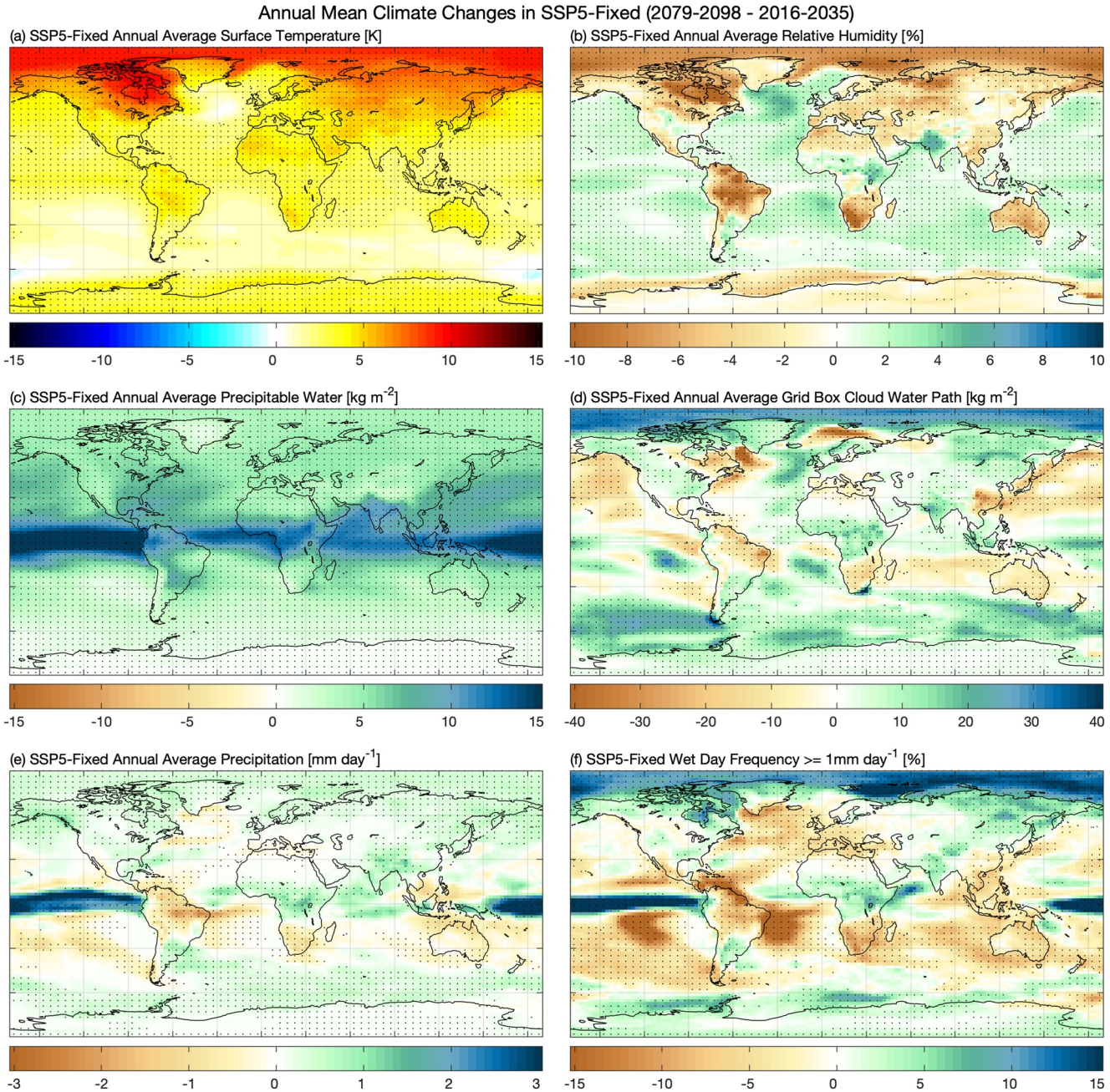

Figure 2. Climate changes [(2079–2098)−(2016–2035)] in the SSP5-Fixed simulation. Annual average surface temperature changes (a) [K], relative humidity at the surface (b) [%], precipitable water (c) [kg/m^2], total grid box cloud liquid water path (d) [kg/m^2], precipitation (e) [mm/day], and wet day frequency (f) which is defined as ≥1 mm/day and converted to units of [%]. Stippling on all subplots indicates statistical significance of these changes at the 99% confidence level.

mean precipitation increases because the occurrence of heavier rates contributes more than moderate rates to the accumulated amount of precipitation (i.e., a small increase in the frequency of rates >10 mm day^{-1} can lead to an overall increase in the precipitation amount) (Figure 3b). Aerosol wet removal has a similar pattern (Figure 3c), but a smaller overall increase of about 1%. The precipitation rates that contribute to the wet deposition amount are lighter than the rates that contribute to the precipitation amount (i.e., the peak in the precipitation amount distribution is about 12 mm day^{-1}, but the peak in the wet deposition amount is about 8 mm day^{-1}), consistent with Wang et al. (2021). Therefore, the change in wet deposition is strongly impacted by the range of precipitation rates that decrease in response to greenhouse gas driven warming. These results demonstrate that, while the

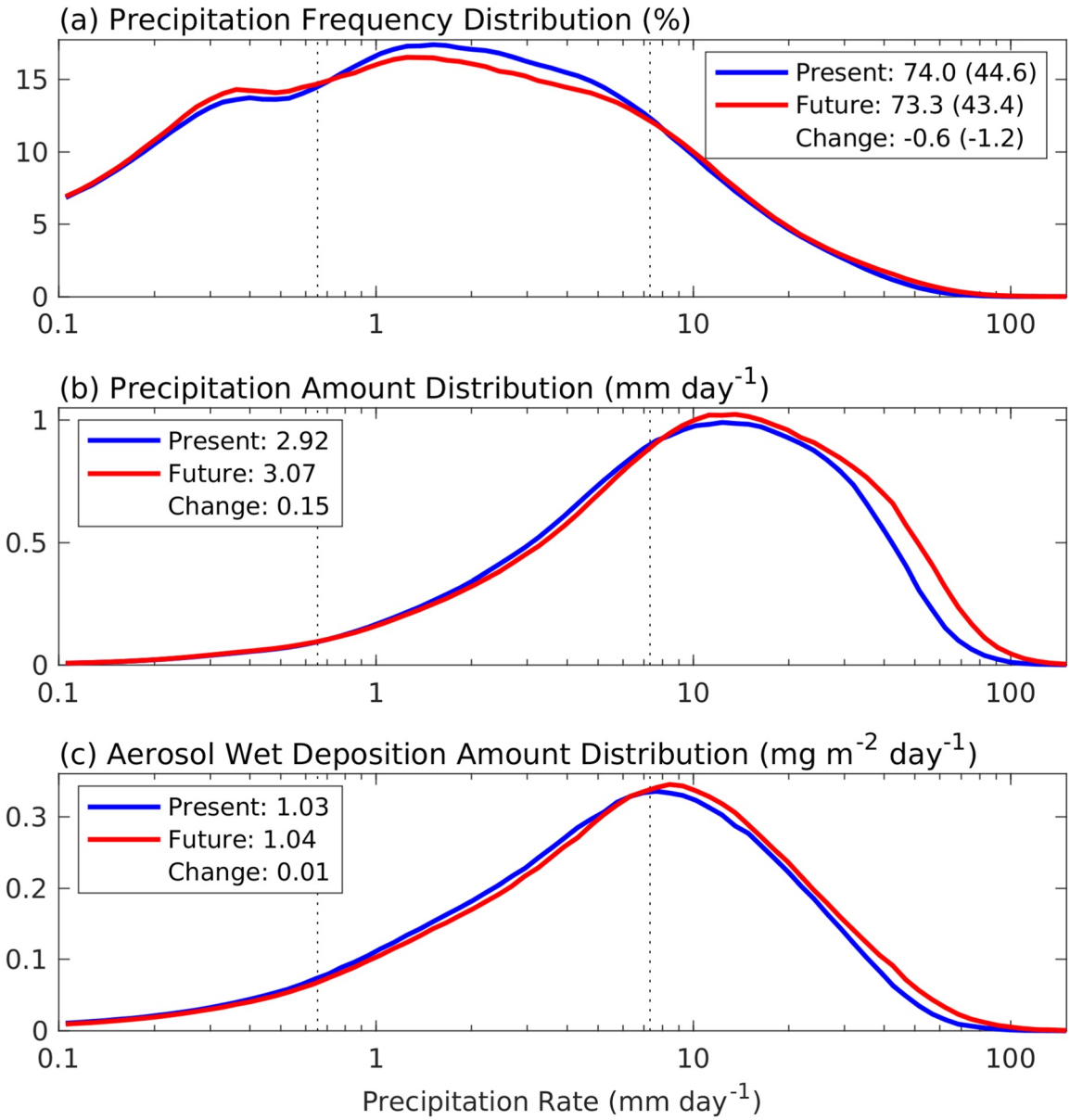

Figure 3. Global mean daily precipitation frequency (a) and amount (b) distributions, as well as wet deposition amount distribution (c) as a function of precipitation rate for the present and future of SSP585-Fixed (assessed with five years of daily output). BC, POM, SO_4, and SOA in all modes are used in wet deposition. Distributions use logarithmic bin spacing ($\Delta \ln R = \Delta R/R = 10\%$) with a 0.1 mm day^{-1} dry-day threshold, similar to Kooperman et al. (2016a, 2016b) and Wang et al. (2021). Numbers in the legend are (a) total frequency of wet days using a threshold of as 0.1 mm day^{-1} (1 mm day^{-1}), (b) total precipitation amount, and (c) total wet removal amount.

overall wet deposition amounts do not change much with warming, removal events occur less frequently and more aerosol is removed per event. This leads to increased aerosol lifetime and higher global mean burdens.

However, a global average view is not sufficient for understanding these potential changes, since area-averages do not assess how regional patterns of precipitation coincide with patterns of aerosol loading over continents (Allen et al., 2015). For example, a strong increase in precipitation over the equator (Figure 2e) does not co-locate with high aerosol burden (Figure S3a in the Supporting Information S1) or regions that are more relevant to air quality concerns. The majority of the global average precipitation increase is centered around the equatorial Pacific, and not likely to contribute to improving air quality in populated areas. In stark contrast, notable regions that experience decreasing rainfall frequency include the majority of South America, southern Africa, and parts of Asia,

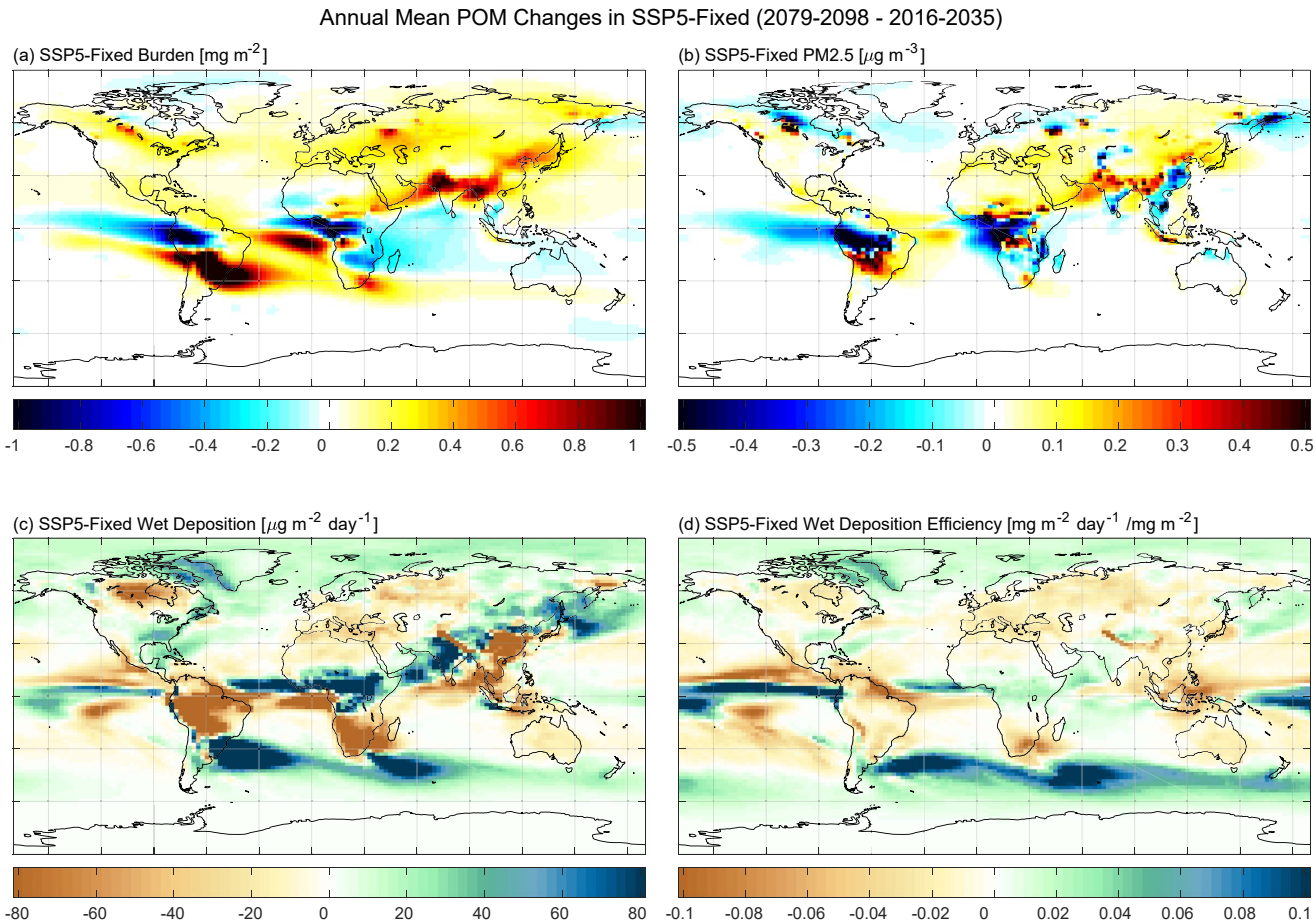

Figure 4. Annual average primary organic matter changes [(2079–2098)−(2016–2035)] for the SSP585-Fixed simulation. Total burden (a) is measured in units of [mg/m^2]. $PM_{2.5}$ at the surface (b) is measured in units of [μg/m^3]. Wet deposition (c) is measured in units of [μg/m^2/day]. Wet deposition efficiency (d) is measured in units of [1/day].

which have higher aerosol burden in the present climate (Figure S3a in the Supporting Information S1) and show strong projected increases in the future (Figure 1a). Additionally, enhanced warming over land in the northern latitudes during summer has been shown to strengthen aerosol pollution through hydrological changes, particularly large-scale precipitation (Allen et al., 2019). We further assess these spatial patterns and their relationship with precipitation for individual aerosol species as changes in the wet deposition efficiency below.

The projected physical climate changes summarized here are consistent with the general features found in the SSP585-Full simulation and across future projections from most modern Earth system models (IPCC, 2013; O'Neill et al., 2016). In the following sections we isolate the impacts of these effects on individual aerosol species.

4.3. Primary Organic Matter and Black Carbon Changes

BC and POM aerosol emissions have many overlapping sources (e.g., combustion of open biomass), and their column burdens and surface concentrations indeed have a similar general pattern for present-day conditions (Figures S7 and S8 in the Supporting Information S1 for BC and POM, respectively). While POM has a stronger signal than BC with larger hotspots in South America and Central Africa, both species generally have higher concentrations over continents, with the largest magnitudes over the tropics and Asia. Likewise, without changes in emissions (i.e., in SSP585-Fixed), similar patterns of burden and surface concentration changes emerge around the tropics for POM (Figure 4) and BC (Figure S9 in the Supporting Information S1). Additionally, both species only have primary production as a source (i.e., no impacts of secondary production), so changes in their mass

can be attributed directly to removal and transport processes. Here we primarily focus on POM, but note that the discussion is relevant to BC as well.

With the sources of POM and BC aerosol fixed at present-day rates, the total sink (wet plus dry deposition) is also fixed in the global mean on climatological timescales (though there may be a temporary decrease on shorter timescales; Xu & Lamarque, 2018), but there can be long-term changes in the partitioning between wet and dry deposition (Table S1 in the Supporting Information S1). As such, an increase in the global burden is primarily associated with an increase in the lifetimes of these aerosols over the 21st century, which increase by 4% and 5% for BC and POM, respectively (Table 1c). These lifetime changes are smaller than that of SOA and SO_4, which are also impacted by secondary production and have different regional relationships with meteorology. In particular, the degree to which aerosol and precipitation changes co-locate can lead to large regional changes that are not evident in the global average. Here we assess the wet deposition efficiency, calculated as the rate of wet deposition relative to the burden of aerosol that is available to be removed (Figure 4d for POM). Changes in the wet deposition efficiency are more widespread than wet deposition itself (Figure 4c vs. 4d) because high (low) deposition coincides with high (low) burdens. This metric of wet deposition efficiency helps to clarify the role of precipitation changes, mapping closely with precipitation frequency (Figure 2f), in the context of changing burdens and transport.

In Figure 4a, there is a strong dipole pattern of burden change evident over South America and Africa, with a decrease to the north and an increase in the south. This pattern results from a combination of changes in removal efficiency and transport, but for different reasons in each region.

Over northern South America, there is an overall decrease in wet deposition (Figures 4c and 4d), which means more POM and BC aerosol can be transported by the background flow. Near the surface, the winds are steered southward by the presence of the Andes Mountains and associated low-level jet (Montini et al., 2019), a circulation pattern that is enhanced at the end of the century (Figures 5a and 5b). This low-level southward flow, in combination with stronger mid-level flow (Figure 5d), leads to reduced (increased) outflow associated with the trade winds to the north (south) over the east Pacific Ocean, and increased outflow by the Southern Hemisphere westerlies to the Atlantic Ocean. This dipole effect is also seen around South Africa, where wet deposition decreases on the continent and increases downwind (Figure 4c) over the ocean to the south, consistent with wind flow changes (Figure 5d).

Over central Africa, there are high present-day values along the west coast just south of the equator (Figure S8a in the Supporting Information S1), and the enhanced mid-level easterly winds off the coast of Angola (Figure 5d) transport more POM and BC aerosol over the Atlantic Ocean. Combined with reduced precipitation (Figures 2e and 2f) and wet deposition (Figures 4c and 4d), this leads to a higher burden around ∼0°–15°S (Figure 4a). However, the high present-day values to the north of the equator are co-located with an increase in precipitation and wet deposition, leading to a lower burden that extends over the equatorial east Atlantic Ocean as less aerosol is carried by the background winds. The effects of increased wet removal also lead to reduced surface concentrations (Figure 4b) that extend along the west coast. Small regional increases in the burden and surface concentration (Figures 4a and 4b) to the north and south of the equatorial reduction over land may be associated with a weakening of the Hadley circulation near the surface (Figure 4b), so less aerosol is removed by transport toward the equator.

Other hotspots of increased POM and BC burden occur over northern India and Asia (Figures 4a and S9 in the Supporting Information S1), which have high present-day values (Figures S7 and S8 in the Supporting Information S1). Over India, despite higher precipitation (Figures 2e and 2f) and wet deposition (Figure 4c), there is an increase in burden. The increase in wet deposition and burden together is associated with minimal wet deposition efficiency changes (Figure 4d) in the region, indicating precipitation is removing more aerosol as the concentration is increasing. Since the aerosol emissions are fixed, this suggests that changes in circulation and transport may be driving the burden changes. In the annual mean, the changes in circulation show more northward flow over India (Figure 5), which contributes to the reduction in surface $PM_{2.5}$ in Southern India and increase to the north. However, this region is strongly influenced by seasonal monsoon changes. When the dry and wet seasons are examined separately, POM burden and surface concentration primarily increase during the dry season (Figure S10a–S10d in the Supporting Information S1). This results from stronger easterly winds that transport aerosols from East Asia and from Southern India (Figure S10e and S10f in the Supporting Information S1),

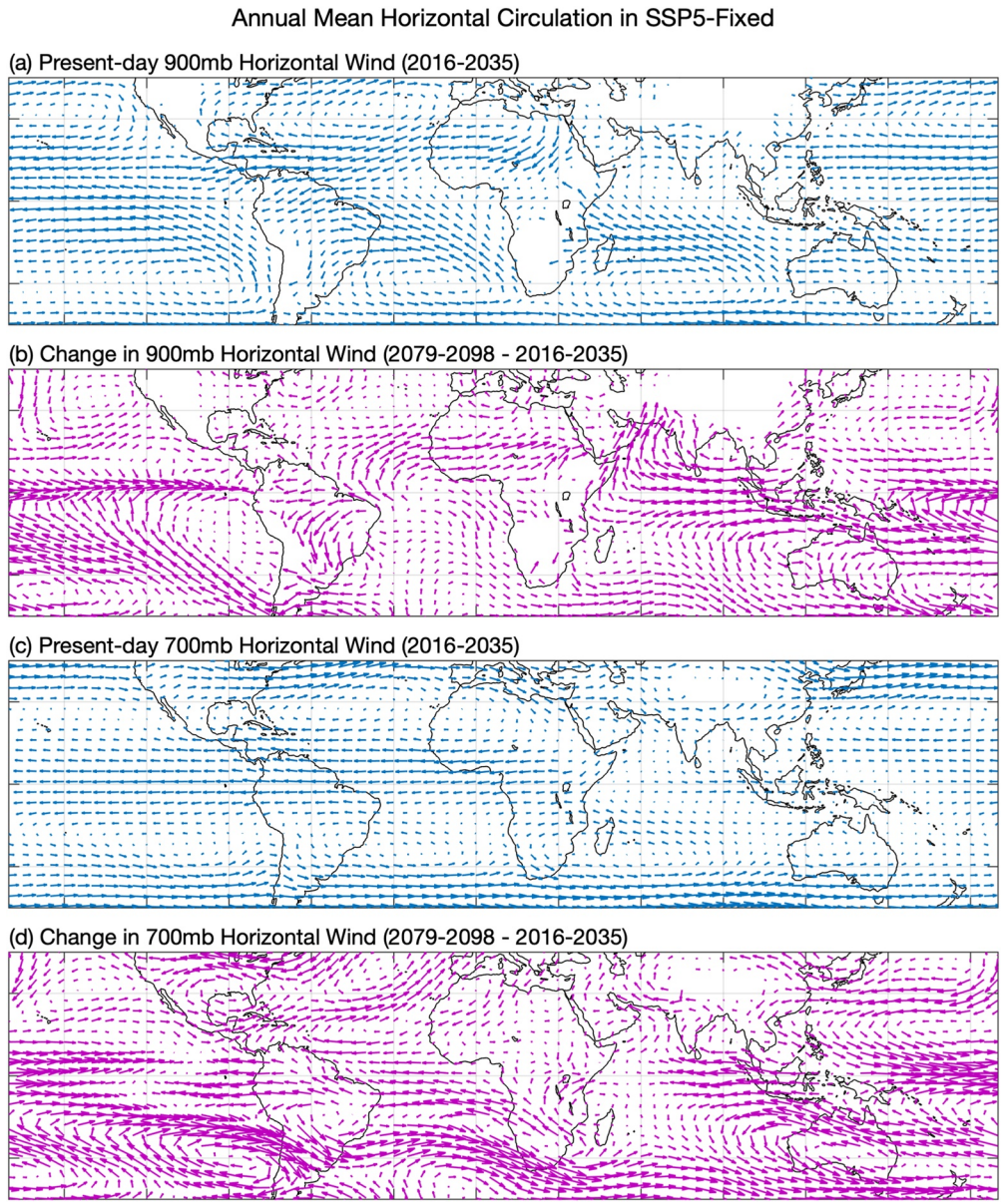

Figure 5. Annual average horizontal wind for (a and c) present-day conditions (2016–2035) and (b and d) changes [(2079–2098)−(2016–2035)] in the SSP585-Fixed simulation at (a and b) 700 mb and (c and d) 900 mb levels. Changes are depicted with arrows 10x larger relative to present-day values.

with a corresponding decrease in the surface concentration in the east. In the wet season, POM is removed both by wet deposition and westerly flow. Over China and Southeast Asia, annual average precipitation frequency (Figure 2f) and wet deposition (Figure 4c) both decline, which contribute to a higher burden. However, surface concentrations show increases to the northwest and decreases to the east, but no obvious causal pattern in the annual mean circulation change. This suggests that an assessment of seasonal changes may be helpful to further unfold contributions to aerosol changes here, though it is not as clear as what we show for India and is beyond the scope of the broad global focus of this work.

Overall, wet deposition efficiency increases in a few small regions (e.g., central Africa), but generally decreases over most continents. This is consistent with a global increase in POM and BC burden, and contributes to longer lifetimes and worsening surface air quality in many regions. However, changes in tropospheric circulation also play an important role in modulating the patterns of aerosol concentrations.

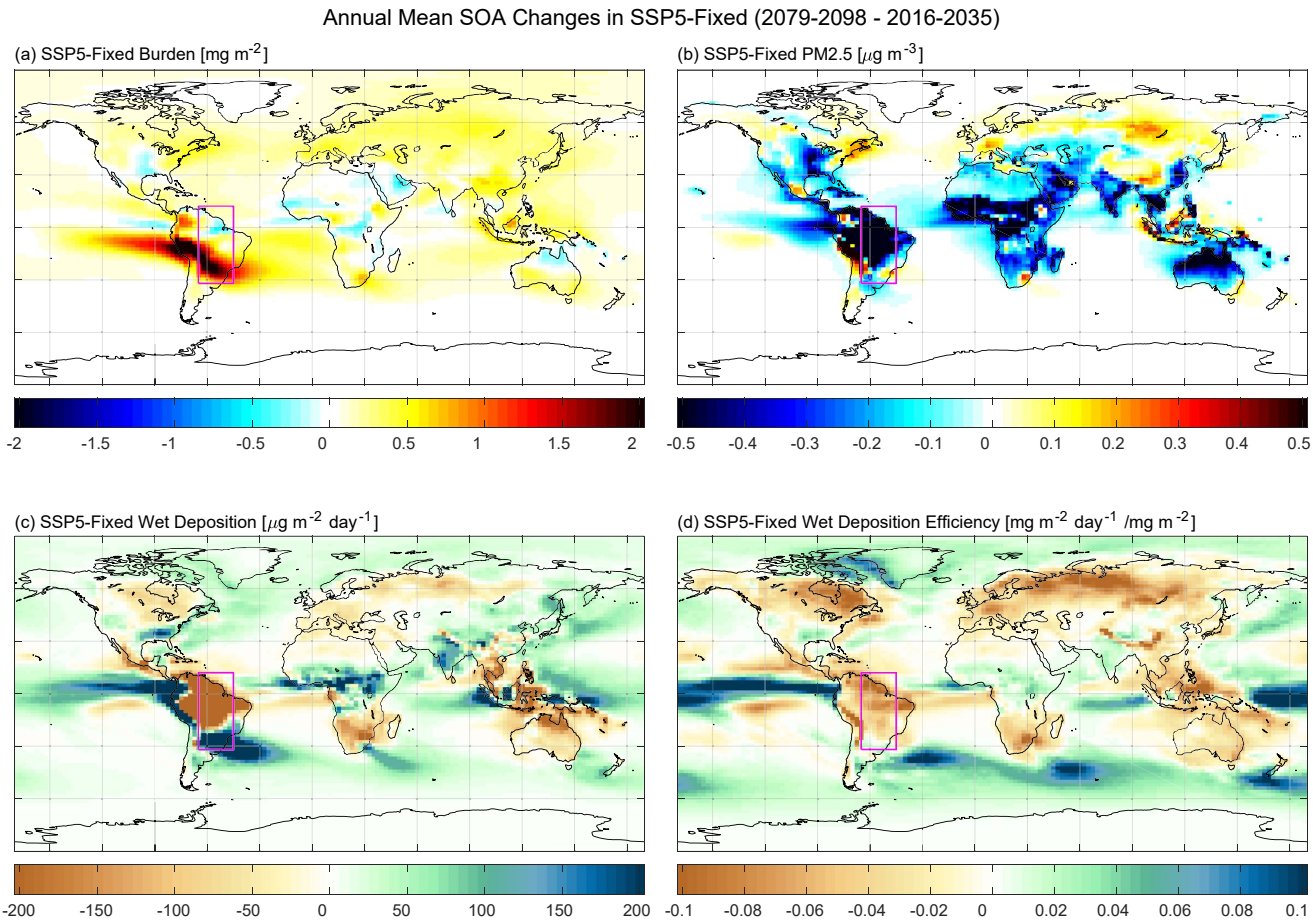

Figure 6. Annual average secondary organic aerosol changes [(2079–2098)−(2016–2035)] in the SSP585-Fixed simulation. Total burden (a) is measured in units of [mg/m^2]. $PM_{2.5}$ at the surface (b) is measured in units of [μg/m^3]. Wet deposition (c) is measured in units of [μg/m^2/day]. Wet deposition efficiency (d) is measured in units of [1/day].

4.4. Secondary Organic Aerosol Changes

While POM, BC, and SO_4 (discussed below in Section 4.5) aerosol species show general agreement between regions with increasing burden and increasing surface $PM_{2.5}$ in the SSP585-Fixed simulation, SOA shows a remarkable disparity between the surface concentration and the atmospheric column burden (Figure 6a vs. 6b). The burden increases broadly over the entire globe, with the largest increase over South America where present-day values are high (Figure S11 in the Supporting Information S1) from biogenic sources (Tilmes et al., 2019). This large-scale increase is reflected in the global average as the highest percent change of all four species (10%; Table 1). Despite this column integrated increase, the surface $PM_{2.5}$ associated with SOA has a large decrease over most land (~6% global average decrease; Table 1). SOA is the only aerosol species with a global mean decrease at the surface, which partly offsets the large SO_4 increase in contributing to the total increase in $PM_{2.5}$ surface concentration.

While there is a small shift from dry to wet deposition of SOA globally (Table S2 in the Supporting Information S1), the general pattern of SOA wet deposition (Figure 6c) is similar to the pattern of POM (Figure 4c), particularly across South America (decrease) and central Africa (increase), as both species have high present-day values in these regions (Figures S8 and S11 in the Supporting Information S1) due to emissions from tropical forests. This indicates that once SOA is formed in the atmosphere (changes in formation are discussed below), it is controlled by the similar transport and removal processes as discussed for POM earlier. For example, over South America wet deposition decreases in the northern half of the continent and increases to the south (Figure 6c). Decreases over the Amazon, associated with reduced rainfall amount and frequency (Figures 2e and 2f), lead to less removal there despite an increase in the burden, while increased removal over Central Africa is associated with

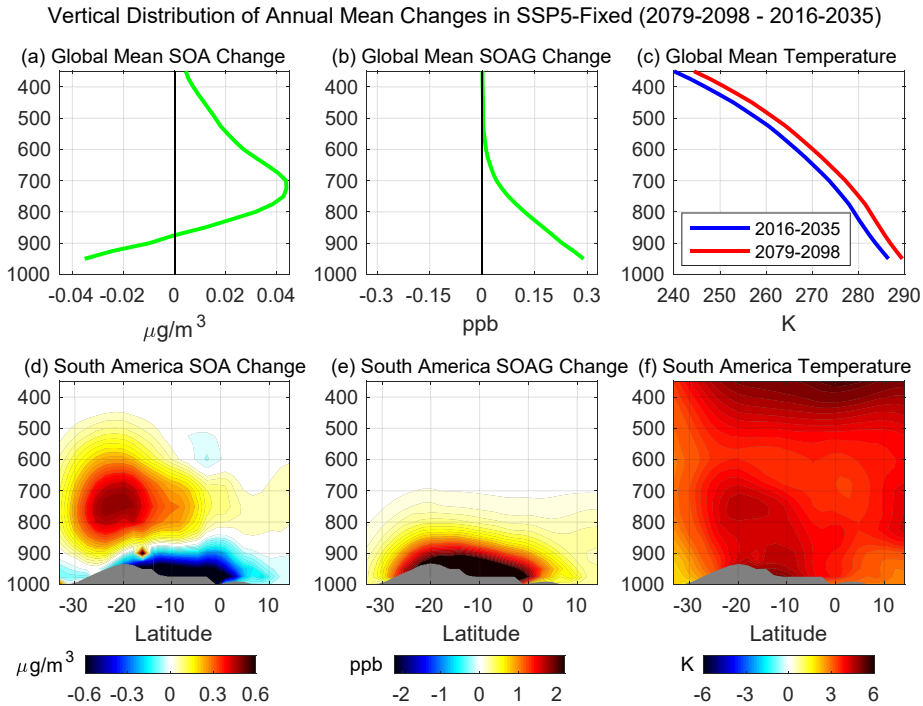

Figure 7. Annual average changes [(2079–2098)−(2016–2035)] in the SSP585-Fixed simulation for vertical profiles of (a and d) SOA (b and e) SOAG, and (c and f) temperature for the (a–c) global mean and (d–f) zonal average cross-section over South America (between 65°W and 45°W).

higher rainfall amount and frequency. This is reflected in the wet deposition efficiency (Figure 6d), which has a large decrease (increase) over northern South America (central Africa) consistent with a reduction (increase) in wet day frequency. Thus, over South America, more aerosol is transported by the background wind away from this region, westward south of the equator and south by the low-level jet into the sub-tropics, leading to higher removal rates downwind where precipitation increases.

However, these changes in removal and transport cannot explain the contrasting decreases at the surface and increases in the burden. While CESM2 has a relatively simple treatment of SOA formation, it does represent the temperature dependence of condensation and evaporation that is missing in many models (Neale et al., 2012), such that SOA formation is influenced by climate changes in the simulation, including surface warming. The disparity between the aerosol concentration in the atmosphere and at the surface, despite no change in emissions, may result from a suppressed production (SOA gas-phase condensation) due to warmer temperatures. As the surface warms, gas-phase constituents will have lower tendency to condense and thus will rise further into cooler air aloft in order to form particle-phase SOA. This is evidenced in the globally averaged vertical profile of SOA (Figure 7a), which shows a decrease at the surface and increase aloft. Consistently, the annual average of SOA precursor gases increases near the surface (SOAG, Figure 7b), despite a fixed emission flux, in the simulated global warming climate (Figure 7c), which tend to increase the saturation vapor pressure of SOA and prolongs the gas-phase.

Focusing on the hot spot of South America (purple box in Figure 6), which has the largest increase in burden, there is a strong decrease in SOA at the surface over the lowland tropical forest (Figure 7d), which coincides with a surface increase in SOAG (Figure 7e). The background wind in this region, characterized by a low-level jet (Montini et al., 2019) is projected to become stronger (Figure 5b), which carries higher SOAG concentrations and warmer air (Figures 7e and 7f) south as it rises out of the region. This enhanced transport contributes to a large upper-level increase in SOA over the region to the south centered at approximately 750 mb. Upper-level zonal winds (Figures 5c and 5d), trade winds to the north and westerlies to the south, then transport SOA leading to the outflow pattern discussed above for the burden and wet deposition.

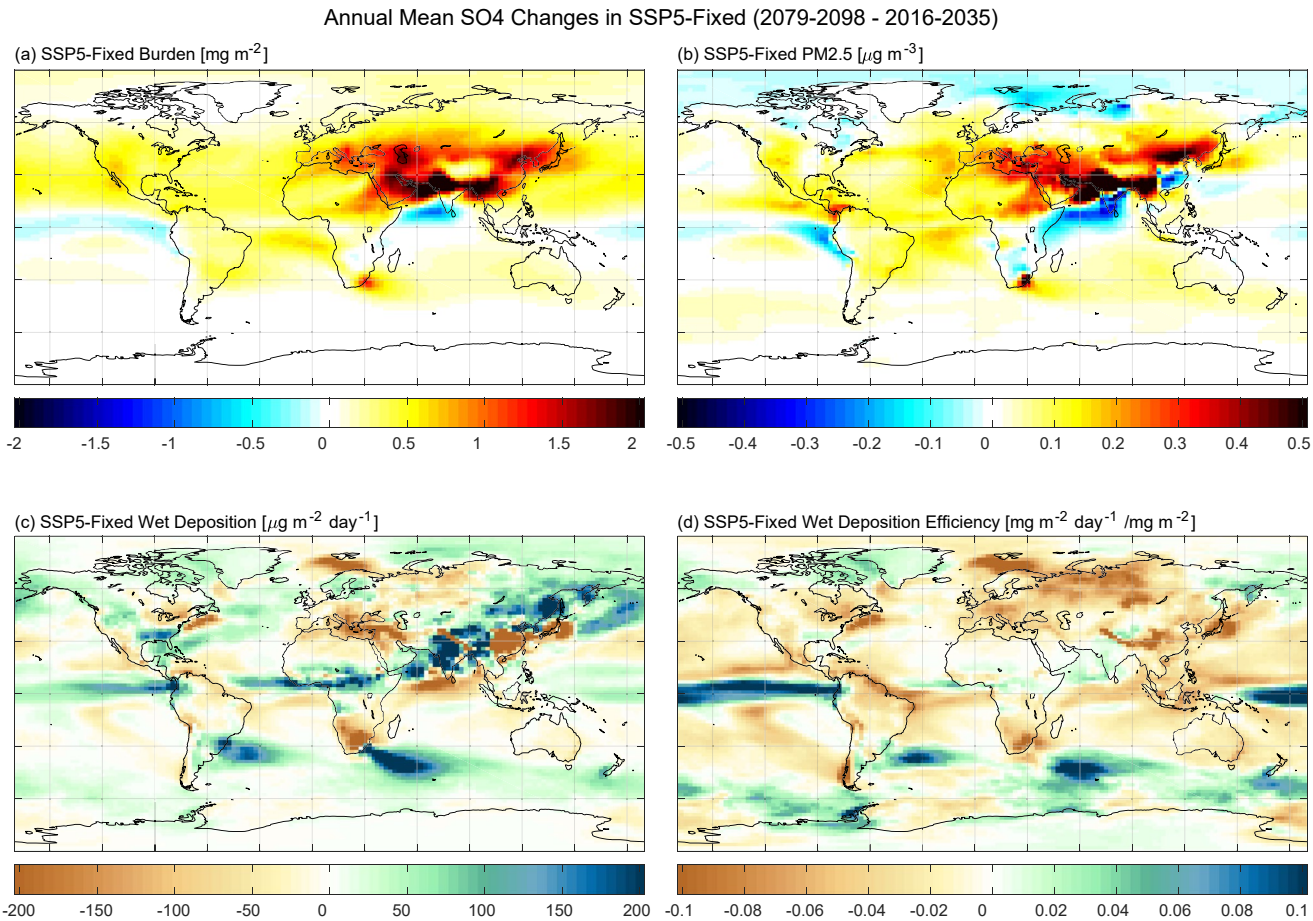

Figure 8. Annual average sulfate changes [(2079–2098)−(2016–2035)] for the SSP585-Fixed simulation. Total burden in all modes (a) are measured in units of [mg/m^2]. $PM_{2.5}$ at the surface (b) is measured in units of [μg/m^3]. Wet deposition (c) is measured in units of [μg/m^2/day]. Wet deposition efficiency (d) is measured in units of [1/day].

To summarize, here we assess changes in SOA with present-day precursor emissions held fixed, which shows overall decreases at the surface, with the exception of the Andes (particularly Peru) and parts of the northern mid-latitudes (e.g., Russia). However, emissions of SOA precursor gas will also be strongly impacted by climate changes, particularly warming over vegetated regions (Lin et al., 2016). These emissions are likely to increase in many regions, which may lead to additional surface level increases that are larger than the reduction identified here due to a suppression in SOA gas-to-particle condensation at the surface. Furthermore, the types and sources of SOA precursors are extremely complex, as are the processes that control the phase changes of different VOCs in the atmosphere, which is not represented in the standard version CESM2's MAM4. Nevertheless, the climate driven changes identified here will likely play an important role in controlling future surface concentrations of SOA, and may partly offset changes that are associated with emissions related processes.

4.5. Sulfate Changes

Assessing the impacts of climate change on sulfate is key for understanding future air quality, as sulfate is projected to increase in concentration at the surface level by 9.3% globally in SSP585-Fixed simulation (Table 1). However, the increases in sulfate are not completely characterized by decreases in precipitation frequency and wet deposition, but are also affected by secondary production in the model (aqueous chemistry and gas-to-aerosol exchange). Though an increase of sulfate concentration in the simulation is seen in most regions (Figure 8), the balance of sources and sinks is complex, despite the emissions of SO_4, SO_2, and DMS remaining fixed at 2010 rates. In the SSP585-Fixed simulation, increasing greenhouse gases and temperature lead to two competing effects. Those effects are (a) sulfate removal changes due to increases or decreases in rainfall frequency that are

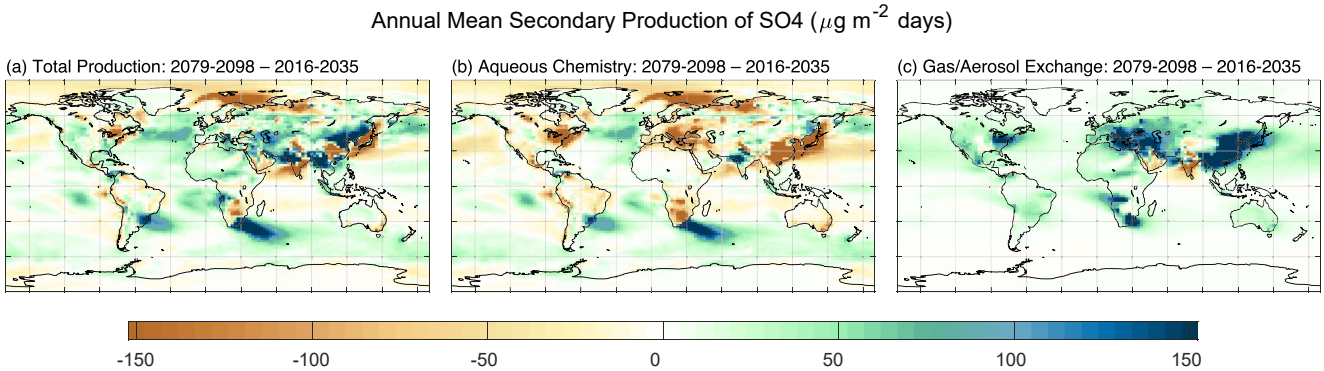

Figure 9. Annual average secondary production of sulfate changes [(2079–2098)−(2016–2035)] in the SSP585-Fixed simulation for (a) total production, (b) aqueous chemistry, and (c) gas-to-aerosol exchange in units of [μg/m^2/days].

location specific, and also (b) the changes in temperature, humidity, and cloud water that governs sulfate production. Both contribute to the patterns of sulfate concentration change (Figure 8) and are examined separately below.

Despite SO_4 aerosol and precursor gas emissions being held at present-day rates, there is an increase in sulfate over all continents, particularly affecting surface concentrations in populated areas (Figures 8a and 8b). These changes amplify the present-day annual mean sulfate burden and surface concentrations, which have the highest values in an arc ranging from Northern Africa to East Asia (Figure S12a and S12b in the Supporting Information S1). Present-day wet deposition is high in similar regions, but is also present on the east coast of North America, Central Africa, and over large portions of Northern Europe and Asia (Figure S12c in the Supporting Information S1). In the SSP585-fixed simulation, fine modes of sulfate at the surface increase over continents similar to the burden, with the exception of East Asia and southern India where it decreases (Figure 8b). This difference at the surface may result in part due to changes in circulation, such as an increase in the easterly wind toward the Arabia Sea and anomalous southerly flow over India (Figure 5). The circulation changes are larger at 900 mb than 700 mb, which may suggest the decrease in SO_4 $PM_{2.5}$ at the surface is affected more by low-level winds, but a smaller upper-level change has less impact on the overall burden.

The primary removal mechanism of sulfate is wet deposition, which, as discussed above, is influenced by physical climate changes in the SSP585-fixed simulation. Sulfate wet deposition increases over areas where concentration increases, such as around South Asia (Figure 8c). However, changes in transport and the production of sulfate also contribute to the concentration change over a given location. For this reason, the wet deposition efficiency metric is particularly useful for understanding how precipitation influences the removal of sulfate with respect to the total burden in the atmosphere (Figure 8d). Deposition efficiency correlates with changes in aerosol lifetime, which has a strong increase of 9% for SO_4 in global mean (Table 1). Furthermore, the wet deposition efficiency decreases consistently over all continents. Regions with large increases in wet deposition (e.g., India) show moderate or little change when viewed through the lens of efficiency changes, suggesting the role of precipitation change is primarily to increase aerosol lifetime.

Total sulfate secondary production results from two types of processes, aqueous chemistry and gas-to-aerosol exchange (Figure 9). In many regions where the total burden increases, it is also boosted by enhancement in gas to aerosol exchange, which leads to increases in total secondary production. Only a few regions have a decrease in gas-phase production (e.g., Arabian Peninsula and southern India), where production through aqueous chemistry increases. Overall, there is a strong inverse relationship between the changes in these two pathways of production (i.e., where there is a decrease in aqueous chemistry, there is an increase in gas-to-aerosol exchange), which is largely dependent on clouds for aqueous production. Decreases (increases) in cloud liquid water (Figure 2d) are associated with decreases (increases) in aqueous chemistry in China (India), and opposite changes in gas-phase production. This is also seen to some extent over South America and southern Africa, where reductions in cloud water (Figure 2d) lead to a decrease in aqueous production. There are some notable regions where a reduction in aqueous production is the larger contribution to the total change (southern Africa and southeast China), but in

general (and in the global mean) gas to aerosol exchange drives an increase in total secondary production by 7.3% (Table S3 in the Supporting Information S1) while the changes in aqueous phase production decreases by 3.1%.

Overall, the pattern of total secondary production change (Figure 9a) is consistent with the annual surface concentration change for SO_4 (Figure 8b). Also, the magnitude of the surface and burden increases tends to be enhanced by a reduction in precipitation frequency and wet deposition efficiency.

5. Conclusions

Due to increasing greenhouse gases in the SSP5-85 scenario, global average precipitation is projected to increase by 4% in our 21st-century GHG-driven simulation. However, the wet day frequency of rainfall decreases by 1.2%, which tends to have a stronger influence on aerosol removal (Hou et al., 2018). This finding is supported by previous studies of precipitation in ESMs, wherein the frequency of light-to-moderate rainfall events are reduced at a global scale (O'Gorman & Schneider, 2009; Pendergrass & Hartmann, 2014a, 2014b; Sun, 2007). When aerosol emissions are fixed with an annual cycle at present-day rates in the SSP585-Fixed simulation, an increasing burden of aerosol is simulated over all continents. There is also an increase in $PM_{2.5}$ at the surface in parts of South America, Europe, and South to East Asia, consistent with previous research suggesting that there is a decrease in wet removal flux over the course of the 21st century, leading to an increased global surface $PM_{2.5}$ concentration (Allen et al., 2015; Xu & Lamarque, 2018). The consistency of these previous studies using CESM1/CAM5/MAM3 and other CMIP5 models with our findings using CESM2/CAM6/MAM4, which has substantial updates in many relevant parameterizations (e.g., convection and aerosols), add confidence to these results. Additionally, we highlight that this is offset by suppressed SOA formation changes across much of the tropics, making the total response across many regions more complex. In this study we provide a comprehensive assessment at the species-level and find that:

1. For BC and POM, whose only source is primary emissions, a combination of precipitation frequency and circulation (mid-to-low level wind flow) changes largely control wet deposition spatial patterns, which lead to regional dipole patterns of increasing and decreasing burden.
2. SOA has a large and spatially consistent increase in global average burden and lifetime when emissions are fixed, but the surface concentration decreases. This remarkable contrast is potentially the result of surface and atmospheric warming, which suppress the SOAG transformation to particles at the surface and effectively shifts the vertical level of SOA production aloft (Figure 7).
3. For SO_4, aqueous and gas phase production are inversely related, and many regions are dominated by higher gas phase formation, increasing the total secondary production (e.g., northern India/Pakistan, Southeast Asia, and northeastern China). In combination with a broad reduction in wet deposition efficiency, most regions show increased burden and surface concentration.
4. Annual mean surface $PM_{2.5}$ concentrations and "Hazardous Air Quality Days" (i.e., days in which $PM_{2.5}$ exceeds 25 $\mu g/m^3$ per WHO daily standards) of the four fixed aerosol species increase in some regions due to meteorological effects alone (physical climate changes). These results, in part due to a general decrease in wet deposition efficiency associated with decreasing precipitation frequency, are evident over land for all aerosol species assessed here.

In this study, we documented the impacts of climate changes on aerosol concentrations over climatological timescales, and highlighted the effects of reduced precipitation frequency. This work was conducted with a conventional ESM (i.e., parameterized convection), which like many modern ESMs (CMIP5/6), tends to under-simulate the intensity and over-simulate the frequency of precipitation (Akinsanola et al., 2020; Kooperman et al., 2018). The results of this study motivate future work in several areas, including analysis of air quality changes on shorter timescales (e.g., seasonal) and applications of models that improve the representation of atmospheric processes (e.g., rainfall characteristics). For example, a seasonal analysis for India (e.g., monsoon rainfall and circulation changes) may further our understanding of the regional changes identified there. India has shown a slowing monsoon season as a result of aerosol interactions in simulations with increased greenhouse gases (Wang et al., 2015), which may affect surface $PM_{2.5}$ concentrations and regional air quality throughout the year. Additionally, CESM2 has the capability to be run with "resolved convection" using a method called super-parameterization (i.e., embedded cloud-resolving models in place of convection and boundary layer parameterizations; Randall et al., 2003) and a stochastic convective parameterization (Wang et al., 2016), both of which have been shown to improve the

representation of precipitation frequency and intensity on global scales (Kooperman et al., 2016b), and may better capture the effects of climate change on aerosol concentrations (Wang et al., 2021).

The results of this study suggest that without future reductions in aerosol emissions, greenhouse-gas driven climate change alone may increase the surface level concentration of fine mode aerosol of multiple species in many regions. These aerosols are hazardous to vulnerable populations and understanding how the regional patterns of these changes coincide with these populations is particularly important for quantifying the global-scale impacts. According to the World Health Organization, the consequences that fall on low- and middle-income countries account for 91% of fine particulate matter deaths due to outdoor aerosol pollution in the current climate (WHO, 2016), and many of these countries have projected reductions in rainfall frequency that may negatively impact their future air quality. Public health planning and mitigation strategies should take into account how both changing aerosol emissions and changes in meteorology may impact future air quality conditions on a regional scale.

Data Availability Statement

Supporting data can be obtained at: All model output necessary to recreate the analysis in this manuscript is available on the U.S. Department of Energy's National Energy Research Scientific Computing Center (https://portal.nersc.gov/archive/home/g/gkooperm/www/Banks_et_al_2021).

Acknowledgments
Development of the Community Earth System Model (CESM) is led by the National Center for Atmospheric Research and is supported by the U.S. National Science Foundation and U.S. Department of Energy (DOE). Gabriel J. Kooperman and Alison Banks acknowledge supported from the U.S. DOE Regional and Global Model Analysis (RGMA) Program (Award Number: DE-SC0019459 and DE-SC0021209) as well as the University of Georgia's Office of Research Junior Faculty Seed Grant and President's Interdisciplinary Seed Grant Programs. Computing resources for this study were provided on the Cheyenne supercomputer by the NSF NCAR Computational Information Systems Laboratory (Project Number: UGAT0001).

References

Akinsanola, A., Kooperman, G. J., Pendergrass, A. G., Hannah, W. M., & Reed, K. A. (2020). Seasonal representation of extreme precipitation indices over the United States in CMIP6 present-day simulations. *Environmental Research Letters*, *15*(10), 094003. https://doi.org/10.1088/1748-9326/ab92c1

Allen, R. J., Hassan, T., Randles, C. A., & Su, H. (2019). Enhanced land-sea warming contrast elevates aerosol pollution in a warmer world. *Nature Climate Change*, *9*, 300–305. https://doi.org/10.1038/s41558-019-0401-4

Allen, R. J., Landuyt, W., & Rumbold, S. T. (2015). An increase in aerosol burden and radiative effects in a warmer world. *Nature Climate Change*, *6*(3), 269–274. https://doi.org/10.1038/nclimate2827

Allen, R. P. & Soden, B. J. (2008). Atmospheric warming and the simplification of precipitation extremes. *Science*, *321*, 1481–1484.

Bogenschutz, P. A., Gettelman, A., Hannay, C., Larson, V. E., Neale, R. B., Craig, C., & Chen, C.-C. (2018). The path to CAM6: Coupled simulations with CAM5.4 and CAM5.5. *Geoscientific Model Development*, *11*, 235–255. https://doi.org/10.5194/gmd-11-235-2018

Bosilovich, M., Cullather, R., & National Center for Atmospheric Research Staff (Eds.), (2019). *The climate data guide: NASA's MERRA2 reanalysis*. Retrieved from https://climatedataguide.ucar.edu/climate-data/nasas-merra2-reanalysis

Chen, H., Wang, H., Sun, J., Xu, Y., & Yin, Z. (2019). Anthropogenic fine particulate matter pollution will be exacerbated in eastern China due to 21st century GHG warming. *Atmospheric Chemistry and Physics*, *19*, 233–243. https://doi.org/10.5194/acp-19-233-2019

Danabasoglu, G., Lamarque, J. F., Bacmeister, J., Bailey, D. A., DuVivier, A. K., Edwards, J., et al. (2020). The community Earth system model version 2 (CESM2). *Journal of Advances in Modeling Earth Systems*, *12*. https://doi.org/10.1029/2019ms001916

Eatough, D. J., Caka, F. M., & Farber, R. J. (1994). The conversion of SO_2 to sulfate in the atmosphere. *Israel Journal of Chemistry*, *34*(3-4), 301–314. https://doi.org/10.1002/ijch.199400034

Emmons, L. K., Schwantes, R. H., Orlando, J. J., Tyndall, G., Kinnison, D., Lamarque, J. F., et al. (2020). The chemistry mechanism in the community Earth system model version 2 (CESM2). *Journal of Advances in Modeling Earth Systems*, *12*(4). https://doi.org/10.1029/2019ms001882

Ervens, B., Turpin, B., & Weber, R. (2011). Secondary organic aerosol formation in cloud droplets and aqueous particles (aqSOA): A review of laboratory, field, and model studies. *Atmospheric Chemistry and Physics*, *11*(21), 11069–11102. https://doi.org/10.5194/acp-11-11069-2011

Feng, W., Wang, M., Zhang, Y., Dai, X., Liu, X., & Xu, Y. (2020). Intraseasonal variation and future projection of atmospheric diffusion conditions conducive to extreme haze formation over eastern China. *Atmospheric and Oceanic Science Letters*, *13*(4), 346–355. https://doi.org/10.1080/16742834.2020.1745054

Gettelman, A., Morrison, H., & Ghan, S. J. (2008). A new two-moment bulk stratiform cloud microphysics scheme in the community atmosphere model, version 3 (CAM3). Part II: Single-column and global results. *Journal of Climate*, *21*, 3660–3679. https://doi.org/10.1175/2008jcli2116.1

Ghan, S. J., Liu, X., Easter, R. C., Zaveri, R., Rasch, P. J., Yoon, J., & Eaton, B. (2012). Toward a minimal representation of aerosols in climate models: Comparative decomposition of aerosol direct, semidirect, and indirect radiative forcing. *Journal of Climate*, *25*(19), 6461–6476. https://doi.org/10.1175/jcli-d-11-00650.1

Gueymard, C. A., & Yang, D. (2020). Worldwide validation of CAMS and MERRA-2 reanalysis aerosol optical depth products using 15 years of AERONET observations. *Atmospheric Environment*, *225*, 117216. https://doi.org/10.1016/j.atmosenv.2019.117216

Hallquist, M., Wenger, J. C., Baltensperger, U., Rudich, Y., Simpson, D., Claeys, M., et al. (2009). The formation, properties and impact of secondary organic aerosol: Current and emerging issues. *Atmospheric Chemistry and Physics*, *9*, 5155–5236. https://doi.org/10.5194/acp-9-5155-2009

Held, I. M., & Soden, B. J. (2006). Robust responses of the hydrological cycle to global warming. *Journal of Climate*, *19*, 5686–5699. https://doi.org/10.1175/jcli3990.1

Hoelzemann, J. J., Longo, K. M., Fonseca, R. M., do Rosário, N. M. E., Elbern, H., Freitas, S. R., & Pires, C. (2009). Regional representativity of AERONET observation sites during the biomass burning season in South America determined by correlation studies with MODIS Aerosol Optical Depth. *Journal of Geophysical Research*, *114*, D13301. https://doi.org/10.1029/2008JD010369

Hong, C., Zhang, Q., Zhang, Y., Davis, S. J., Tong, D., Zheng, Y., et al. (2019). Impacts of climate change on future air quality and human health in China. *Proceedings of the National Academy of Sciences*, 116(35), 17193–17200. https://doi.org/10.1073/pnas.1812881116

Hou, P., Wu, S., Mccarty, J. L., & Gao, Y. (2018). Sensitivity of atmospheric aerosol scavenging to precipitation intensity and frequency in the context of global climate change. *Atmospheric Chemistry and Physics*, *18*(11), 8173–8182. https://doi.org/10.5194/acp-18-8173-2018

Huffman, G. J., Bolvin, D. T., & Adler, R. F. (2016). GPCP Version 1.2 One-Degree Daily Precipitation Data Set [dataset]. Research Data Archive at the National Center for Atmospheric Research, Computational and Information Systems Laboratory. https://doi.org/10.5065/D6D50K46

Iacono, M. J., Delamere, J. S., Mlawer, E. J., Shephard, M. W., Clough, S. A., & Collins, W. D. (2008). Radiative forcing by long-lived greenhouse gases: Calculations with the AER radiative transfer models. *Journal of Geophysical Research*, *113*, D13103. https://doi.org/10.1029/2008JD009944

IPCC. (2013). In T. F. Stocker, D. Qin, G. K. Plattner, M. Tignor, S. K. Allen, J. Boschung, et al. (Eds.), *Climate change 2013: The physical science basis. Contribution of working group I to the fifth assessment report of the intergovernmental panel on climate change*. 1535, Cambridge University Press.

Keene, W. C., Galloway, J. N., Likens, G. E., Deviney, F. A., Mikkelsen, K. N., Moody, J. L., & Maben, J. R. (2015). Atmospheric wet deposition in remote regions: Benchmarks for environmental change. *Journal of the Atmospheric Sciences*, *72*(8), 2947–2978. https://doi.org/10.1175/JAS-D-14-0378.1

Kooperman, G. J., Pritchard, M. S., Burt, M. A., Branson, M. D., & Randall, D. A. (2016a). Impacts of cloud superparameterization on projected daily rainfall intensity climate changes in multiple versions of the Community Earth System Model. *Journal of Advances in Modeling Earth Systems*, *8*, 1727–1750. https://doi.org/10.1002/2016MS000715

Kooperman, G. J., Pritchard, M. S., Burt, M. A., Branson, M. D., & Randall, D. A. (2016b). Robust effects of cloud superparameterization on simulated daily rainfall intensity statistics across multiple versions of the Community Earth System Model. *Journal of Advances in Modeling Earth Systems*, *8*, 140–165. https://doi.org/10.1002/2015MS000574

Kooperman, G. J., Pritchard, M. S., O'Brien, T. A., & Timmermans, B. W. (2018). Rainfall from resolved rather than parameterized processes better represents the present-day and climate change response of moderate rates in the community atmosphere model. *Journal of Advances in Modeling Earth Systems*, *10*, 971–988. https://doi.org/10.1002/2017MS001188

Kroll, J., Ng, N. L., Murphy, S. M., Flagan, R. C., & Seinfeld, J. H. (2006). Secondary organic aerosol formation from Isoprene photooxidation. *Environmental Science & Technology*, *40*(6), 1869–1877. https://doi.org/10.1021/es0524301

Lamarque, J. F., Bond, T. C., Eyring, V., Granier, C., Heil, A., Klimont, Z., et al. (2010). Gridded anthropogenic and biomass burning emissions of reactive gases and aerosols: Methodology and application. *Atmospheric Chemistry and Physics*, *10*, 7017–7039, 49635019. https://doi.org/10.5194/acp-10-7017-2010

Lamarque, J. F., Shindell, D. T., Josse, B., Young, P. J., Cionni, I., Eyring, V., et al. (2013). The atmospheric chemistry and climate model intercomparison Project (ACCMIP): Overview and description of models, simulations and climate diagnostics. *Geoscientific Model Development*, *6*, 179–206. https://doi.org/10.5194/gmd-6-179-2013

Lin, G., Penner, J. E., & Zhou, C. (2016). How will SOA change in the future? *Geophysical Research Letters*, *43*, 1718–1726. https://doi.org/10.1002/2015GL067137

Liu, X., Easter, R. C., Ghan, S. J., Zaveri, R., Rasch, P., Shi, X., et al. (2012). Toward a minimal representation of aerosols in climate models: Description and evaluation in the community atmosphere model CAM5. *Geoscientific Model Development*, *5*(3), 709–739. https://doi.org/10.5194/gmd-5-709-2012

Liu, X., Ma, P.-L., Wang, H., Tilmes, S., Singh, B., Easter, R. C., et al. (2016). Description and evaluation of a new four-mode version of the modal aerosol module (MAM4) within version 5.3 of the community atmosphere model. *Geoscientific Model Development*, *9*(2), 505–522. https://doi.org/10.5194/gmd-9-505-2016

Lynch, J. A., Bowersox, V. C., & Grimm, J. W. (2000). Changes in sulfate deposition in eastern USA following implementation of phase I of title IV of the clean air act amendments of 1990. *Atmospheric Environment*, *34*(11), 1665–1680. https://doi.org/10.1016/S1352-2310(99)00426-4

Montini, T. L., Jones, C., & Carvalho, L. M. V. (2019). The South American low-level jet: A new climatology, variability, and changes. *Journal of Geophysical Research: Atmospheres*, *124*, 1200–1218. https://doi.org/10.1029/2018JD029634

Neale, R. B., Chen, C. C., Gettelman, A., Lauritzen, P. H., Park, S., Williamson, D. L., et al. (2012). Description of the NCAR community atmosphere model (CAM 5.0). *NCAR Tech Note NCAR/TN486STR1274*, (Vol. 1). p. 274, National Center for Atmospheric Research.

O'Gorman, P. A., & Schneider, T. (2009). The physical basis for increases in precipitation extremes in simulations of 21st-century climate change. In *Proceedings of the National Academy of Sciences* (Vol. 106, pp. 14773–14777). https://doi.org/10.1073/pnas.0907610106

O'Neill, B. C., Tebaldi, C., van Vuuren, D. P., Eyring, V., Friedlingstein, P., Hurtt, G., et al. (2016). The scenario model intercomparison Project (ScenarioMIP) for CMIP6. *Geoscientific Model Development*, *9*(9), 3461–3482. https://doi.org/10.5194/gmd-9-3461-2016

Park, S., Allen, R. J., & Lim, C. H. (2020). A likely increase in fine particulate matter and premature mortality under future climate change. *Air Quality, Atmosphere & Health*, *13*, 143–151. https://doi.org/10.1007/s11869-019-00785-7

Pendergrass, A., & National Center for Atmospheric Research Staff (Eds.), (2016). *The climate data guide: GPCP (daily): Global precipitation climatology project*. Retrieved from http://climatedataguide.ucar.edu/climate-data/gpcp-daily-global-precipitation-climatology-project

Pendergrass, A. G., & Hartmann, D. L. (2014a). The atmospheric energy constraint on global-mean precipitation. *Journal of Climate*, *27*, 757–768. https://doi.org/10.1175/jcli-d-13-00163.1

Pendergrass, A. G., & Hartmann, D. L. (2014b). Changes in the distribution of rain frequency and intensity in response to global warming. *Journal of Climate*, *27*, 8372–8383. https://doi.org/10.1175/JCLI-D-14-00183.1

Poeschl, U. (2006). Atmospheric aerosols: Composition, transformation, climate and health effects. *ChemInform*, *37*(7). https://doi.org/10.1002/chin.200607299

Polade, S., Pierce, D., Cayan, D., Gershunov, A., & Dettinger, M. D. (2014). The key role of dry days in changing regional climate and precipitation regimes. *Scientific Reports*, *4*, 4364. https://doi.org/10.1038/srep04364

Randall, D., Khairoutdinov, M., Arakawa, A., & Grabowski, W. (2003). Breaking the cloud parameterization deadlock. *Bulletin of the American Meteorological Society*, *84*(11), 1547–1564. https://doi.org/10.1175/BAMS-84-11-1547

Roldán-Henao, N., Hoyos, C. D., Herrera-Mejía, L., & Isaza, A. (2020). An investigation of the precipitation net effect on the particulate matter concentration in a narrow valley: Role of lower-Troposphere stability. *Journal of Applied Meteorology and Climatology*, *59*(3), 401–426. https://doi.org/10.1175/JAMC-D-18-0313.1

Scott, W. D., & Hobbs, P. V. (1967). The formation of sulfate in water droplets. *Journal of the Atmospheric Sciences*, *24*(1), 54–57. https://doi.org/10.1175/1520-0469(1967)024<0054:tfosiw>2.0.co;2

Seidel, D. J., Fu, Q., Randel, W. J., & Reichler, T. J. (2008). Widening of the tropical belt in a changing climate. *Nature Geoscience*, *1*, 21–24. https://doi.org/10.1038/ngeo.2007.38

Shi, H., Xiao, Z., Zhan, X., Ma, H., & Tian, X. (2019). Evaluation of MODIS and two reanalysis aerosol optical depth products over AERONET sites. *Atmospheric Research*, *220*, 75–80. https://doi.org/10.1016/j.atmosres.2019.01.009

Shrivastava, M., Cappa, C. D., Fan, J., Goldstein, A. H., Guenther, A. B., Jimenez, J. L., et al. (2017). Recent advances in understanding secondary organic aerosol: Implications for global climate forcing. *Reviews of Geophysics*, *55*, 509–559. https://doi.org/10.1002/2016RG000540

Sickles, J. E., & Shadwick, D. S. (2007). Changes in air quality and atmospheric deposition in the Eastern United States (1990 – 2000). *Journal of Geophysical Research: Atmospheres*, *112*, D17302. https://doi.org/10.1029/2006JD008356

Silva, R. A., West, J. J., Lamarque, J.-F., Shindell, D. T., Collins, W. J., Dalsoren, S., et al. (2016). The effect of future ambient air pollution on human premature mortality to 2100 using output from the ACCMIP model ensemble. *Atmospheric Chemistry and Physics*, *16*, 9847–9862. https://doi.org/10.5194/acp-16-9847-2016

Silva, R. A., West, J. J., Lamarque, J.-F., Shindell, D. T., Collins, W. J., Faluvegi, G., et al. (2017). Future global mortality from changes in air pollution attributable to climate change. *Nature Climate Change*, *7*, 647–651. https://doi.org/10.1038/NCLIMATE3354

Smith, S. J., Zhou, Y., Kyle, P., Wang, H., & Yu, H. (2015). A community emissions data system (CEDS): Emissions for CMIP6 and beyond. In *Proceedings of the 2015 International emission Inventory Conference* (pp. 12–16).

Sun, Y., Solomon, S., Dai, A., & Portmann, R. W. (2007). How often will it rain? *Journal of Climate*, *20*(19), 4801–4818. https://doi.org/10.1175/jcli4263.1

Teixeira, J., Waliser, D., Ferraro, R., Gleckler, P., Lee, T., & Potter, G. (2014). Satellite observations for CMIP5: The Genesis of Obs4MIPs. *Bulletin of the American Meteorological Society*, *95*(9), 1329–1334. https://doi.org/10.1175/bams-d-12-00204.1

Tie, X., Brasseur, G., Emmons, L., Horowitz, L., & Kinnison, D. (2001). Effects of aerosols on tropospheric oxidants: A global model study. *Journal of Geophysical Research*, *106*(D19), 22931–22964. https://doi.org/10.1029/2001jd900206

Tilmes, S., Hodzic, A., Emmons, L. K., Mills, M. J., Gettelman, A., Kinnison, D. E., et al. (2019). Climate forcing and trends of organic aerosols in the community Earth system model (CESM2). *Journal of Advances in Modeling Earth Systems*, *11*(12), 4323–4351. https://doi.org/10.1029/2019MS001827

van Donkelaar, A., Martin, R. V., Brauer, M., Hsu, N. C., Kahn, R. A., Levy, R. C., et al. (2018). *Global annual $PM_{2.5}$ grids from MODIS, MISR and SeaWiFS aerosol optical depth (AOD) with GWR, 1998–2016*. NASA Socioeconomic Data and Applications Center (SEDAC). https://doi.org/10.7927/H4ZK5DQS

Vet, R., Artz, R. S., Carou, S., Shaw, M., Ro, C.-U., Aas, W., et al. (2014). A global assessment of precipitation chemistry and deposition of sulfur, nitrogen, sea salt, base cations, organic acids, acidity and pH, and phosphorus. *Atmospheric Environment*, *93*, 3–100. https://doi.org/10.1016/j.atmosenv.2013.10.060

Wang, Y., Jiang, J. H., & Su, H. (2015). Atmospheric responses to the redistribution of anthropogenic aerosols. *Journal of Geophysical Research: Atmospheres*, *120*(18), 9625–9641. https://doi.org/10.1002/2015jd023665

Wang, Y., Xia, W., Liu, X., Xie, S., Lin, W., Tang, Q., et al. (2021). Disproportionate control on aerosol burden by light rain. *Nature Geoscience*, *14*, 72–76. https://doi.org/10.1038/s41561-020-00675-z

Wang, Y., Zhang, G. J., & Craig, G. C. (2016). Stochastic convective parameterization improving the simulation of tropical precipitation variability in the NCAR CAM5. *Geophysical Research Letters*, *43*, 6612–6619. https://doi.org/10.1002/2016gl069818

Wang, Z., Lin, L., Zhang, X., Zhang, H., Liu, L., & Xu, Y. (2017). Scenario dependence of future changes in climate extremes under 1.5°C and 2°C global warming. *Scientific Reports*, *7*, 46432. https://doi.org/10.1038/srep46432

World Health Organization. (2016). *Ambient air pollution: A global assessment of exposure and burden of disease*. Retrieved from http://www.who.int/iris/handle/10665/250141

Wu, X., Xu, Y., Kumar, R., & Barth, M. (2019). Separating emission and meteorological drivers of mid-21st-century air quality changes in India based on multiyear global-regional chemistry-climate simulations. *Journal of Geophysical Research: Atmospheres*, *124*, 13420–13438. https://doi.org/10.1029/2019JD030988

Xu, Y., & Lamarque, J. (2018). Isolating the meteorological impact of 21st century GHG warming on the removal and atmospheric loading of anthropogenic fine particulate matter pollution at global scale. *Earth's Future*, *6*(3), 428–440. https://doi.org/10.1002/2017ef000684

Xu, Y., Wu, X., Kumar, R., Barth, M., Diao, C., Gao, M., et al. (2020). Substantial increase in the joint occurrence and human exposure of heatwave and high-PM hazards over South Asia in the mid-21st century. *AGU Advances*, *1*, e2019AV000103. https://doi.org/10.1029/2019AV000103

Yang, J., Kang, S., Ji, Z., Tripathee, L., Yin, X., & Yang, R. (2020). Investigation of variations, causes and component distributions of $PM_{2.5}$ mass in China using a coupled regional climate-chemistry model. *Atmospheric Pollution Research*, *11*(2), 319–331. https://doi.org/10.1016/j.apr.2019.11.005

Yin, J. H. (2005). A consistent poleward shift of the storm tracks in simulations of 21st century climate. *Geophysical Research Letters*, *32*(18). https://doi.org/10.1029/2005GL023684

Zhang, Q., Xue, D., Liu, X., Gong, X., & Gao, H. (2019). Process analysis of $PM_{2.5}$ pollution events in a coastal city of China using CMAQ. *Journal of Environmental Sciences*, *79*, 225–238. https://doi.org/10.1016/j.jes.2018.09.007